

# Investigating the role of new physics in $b \rightarrow c\tau\bar{\nu}_\tau$ transitions

Suchismita Sahoo<sup>1,\*</sup> and Rukmani Mohanta<sup>2,†</sup>

<sup>1</sup> *Theoretical Physics Division, Physical Research Laboratory, Ahmedabad-380009, India*

<sup>2</sup> *School of Physics, University of Hyderabad, Hyderabad - 500046, India*

## Abstract

In recent times, the charged-current mediated semileptonic  $b \rightarrow c\tau\bar{\nu}_\tau$  processes have attracted a lot of attention after the observation of lepton non-universality ratios,  $R_{D^{(*)}}$ ,  $R_{J/\psi}$  and the measurements on  $D^*$  and  $\tau$  longitudinal polarization fractions in  $\bar{B} \rightarrow D^*\tau\bar{\nu}_\tau$  processes. We present a model-independent analysis of  $\bar{B} \rightarrow D^{(*)}\tau\bar{\nu}_\tau$ ,  $B_s \rightarrow D_s^{(*)}\tau\bar{\nu}_\tau$ ,  $B_c^+ \rightarrow (\eta_c, J/\psi)\tau^+\nu_\tau$ ,  $\Lambda_b \rightarrow \Lambda_c\tau\bar{\nu}_\tau$  and  $\bar{B} \rightarrow D^{**}\tau\bar{\nu}_\tau$  (where  $D^{**} = \{D_0^*, D_1^*, D_1, D_2^*\}$  are the four lightest excited charm mesons) processes involving  $b \rightarrow c\tau\bar{\nu}$  quark level transitions by considering the most general effective Lagrangian in the presence of new physics. We perform a global fit to various set of new coefficients, including the measurements on  $R_{D^{(*)}}$ ,  $R_{J/\psi}$  and the upper limit on  $\text{Br}(B_c^+ \rightarrow \tau^+\bar{\nu}_\tau)$ . We then show the implications of constrained new couplings on the branching fractions, lepton non-universality ratios and various angular observables of these decay modes in four different bins of  $q^2$ .

---

\*Electronic address: suchismita8792@gmail.com

†Electronic address: rukmani98@gmail.com

## I. INTRODUCTION

Although, we have not seen any unambiguous signal of new physics (NP) at the LHC experiment so far, the observation of lepton universality violating (LUV) ratios in  $b \rightarrow sll$  ( $R_{K^{(*)}}$ ) [1–4] and  $b \rightarrow c\tau\bar{\nu}_\tau$  ( $R_{D^{(*)}}$ ,  $R_{J/\psi}$ ) [5–16] decay modes have provided an indirect hint for the existence of NP beyond the Standard Model (SM). The measurements on lepton non-universality (LNU) observables,  $R_K \equiv \Gamma(B^+ \rightarrow K^+ \mu^+ \mu^-)/\Gamma(B^+ \rightarrow K^+ e^+ e^-)$  along with  $R_{K^*} \equiv \Gamma(B^0 \rightarrow K^{*0} \mu^+ \mu^-)/\Gamma(B^0 \rightarrow K^{*0} e^+ e^-)$  by LHCb Collaborations disagree with their SM predictions at  $\sim 2.5\sigma$  level [1–4, 17, 18]. In the  $b \rightarrow c\tau\bar{\nu}_\tau$  sector, the LHCb [10–13] as well as Belle [5–9] and BaBar [14, 15] have measured the LNU ratios,  $R_{D^{(*)}} \equiv \Gamma(\bar{B} \rightarrow D^{(*)} \tau\bar{\nu}_\tau)/\Gamma(\bar{B} \rightarrow D^{(*)} l\bar{\nu}_l)$  and  $R_{J/\psi} \equiv \Gamma(B_c^+ \rightarrow J/\psi \tau^+ \nu_\tau)/\Gamma(B_c^+ \rightarrow J/\psi l^+ \nu_l)$ , where  $l = e, \mu$ . Combining the  $R_{D^{(*)}}$  data of all the experiments, the world average values by HFLAV Collaboration [16] are

$$R_D^{\text{Expt}} = 0.340 \pm 0.027 \pm 0.013, \quad R_{D^*}^{\text{Expt}} = 0.295 \pm 0.011 \pm 0.008, \quad (1)$$

which disagree with their SM predictions [19–21]

$$R_D^{\text{SM}} = 0.299 \pm 0.003, \quad R_{D^*}^{\text{SM}} = 0.258 \pm 0.005, \quad (2)$$

by  $3.08\sigma$ . The measured value of  $R_{J/\psi}$  by LHCb [10]

$$R_{J/\psi}^{\text{Expt}} = 0.71 \pm 0.17 \pm 0.18, \quad (3)$$

also shows a  $1.7\sigma$  deviation from the corresponding SM prediction [22–24]

$$R_{J/\psi}^{\text{SM}} = 0.289 \pm 0.01. \quad (4)$$

The uncertainties from the CKM matrix elements and the form factors are canceled out to a large extent in all these LNU ratios associated with  $b \rightarrow sll$  and  $b \rightarrow c\tau\bar{\nu}_\tau$  and hence, these observed anomalies indirectly point towards the possible interplay of new physics. Besides these LNU ratios, the Belle Collaboration has also measured  $D^*$  and  $\tau$  longitudinal polarization fractions in  $\bar{B} \rightarrow D^* \tau\bar{\nu}_\tau$  channel. The measured values of  $P_\tau^{D^*}$  by Belle [9]

$$P_\tau^{D^*} |^{\text{Expt}} = -0.38 \pm 0.51^{+0.21}_{-0.16}, \quad (5)$$

is almost consistent with its SM prediction,  $P_\tau^{D^*}|^{\text{SM}} = -0.497 \pm 0.013$  [25]. However, disagreement of  $1.6\sigma$  is found between the Belle measurement [26, 27]

$$F_L^{D^*} |^{\text{Expt}} = 0.60 \pm 0.08 \pm 0.04, \quad (6)$$

and its SM prediction,  $F_L^{D^*}|_{\text{SM}} = 0.46 \pm 0.04$  [28].

The investigation of charge-current mediated semileptonic decays like  $\bar{B} \rightarrow D^{(*)}\tau\bar{\nu}_\tau$ ,  $B_s \rightarrow D_s^{(*)}\tau\bar{\nu}_\tau$ ,  $B_c^+ \rightarrow (\eta_c, J/\psi)\tau^+\nu_\tau$ ,  $\Lambda_b \rightarrow \Lambda_c\tau\bar{\nu}_\tau$  and  $\bar{B} \rightarrow D^{**}\tau\bar{\nu}_\tau$  driven by  $b \rightarrow c\tau\bar{\nu}_\tau$  transition are utterly interesting, as the NP contributions would have to be significantly large enough to provide visible impact in these tree level decay channels in the SM, which in turn would require new particles to be either rather light or strongly coupled to the SM particles. Both the decay processes  $\bar{B} \rightarrow D^{(*)}$  and  $B_s \rightarrow D_s^{(*)}$  are related by  $SU(3)$  flavor symmetry, i.e., differ only in their spectator quark, mediated by  $b \rightarrow c$  transition, involving the same CKM matrix element  $V_{cb}$ . Therefore, a detailed comprehensive analysis of these channels will help in determining the value of  $|V_{cb}|$ . The semileptonic decays of  $B_{(s)}$  and  $B_c$  mesons have been studied intensively in the literature [29–41]. The heavy-heavy baryonic decay modes of  $b$ -flavored baryons can also serve as an additional source for the determination of the CKM matrix element  $V_{cb}$  [42–45], which are investigated by many authors in the SM as well as in the presence of NP [46–59]. In Ref. [60, 61], the rare semileptonic decays of  $B$  meson to higher excited charmed mesons ( $D^{**}$ ) with a lepton and a neutrino in the final state i.e.,  $\bar{B} \rightarrow D^{**}l\bar{\nu}_l$ , where  $D^{**} \in D_0^*, D_1^*, D_1, D_2$  are scrutinized in the SM and in the model independent approach. In this work, we would like to study all the above discussed decay processes involving  $b \rightarrow c\tau\bar{\nu}_\tau$  quark level transition in a model independent way by extending the operator structure of Lagrangian beyond standard model. In this approach, we find additional Wilson coefficients contributions to the SM coefficients. We constrain the new parameters from the  $\chi^2$  fit of  $R_{D^{(*)}}$ ,  $R_{J/\psi}$  and upper limit on  $\text{Br}(B_c^+ \rightarrow \tau^+\nu_\tau)$ . The bin-wise branching ratio, forward-backward asymmetry, LNU ratios,  $\tau$  and  $V(= D_{(s)}^*, J/\psi)$  polarization asymmetry of  $b \rightarrow c\tau\bar{\nu}_\tau$  decay modes for both real and complex new coefficients are estimated in this analysis.

The plan of the paper is as follows. In section II, we give the most general interaction Lagrangian and the theoretical framework for the analysis of  $b \rightarrow c\tau\bar{\nu}_\tau$  transition. Our methodology to constrain the new coefficients is presented in section III. Section IV describes the bin-wise numerical analysis of branching ratios and various angular observables of  $\bar{B} \rightarrow D^{(*)}\tau\bar{\nu}_\tau$ ,  $B_s \rightarrow D_s^{(*)}\tau\bar{\nu}_\tau$ ,  $B_c^+ \rightarrow (\eta_c, J/\psi)\tau^+\nu_\tau$  decay processes. The  $\Lambda_b \rightarrow \Lambda_c\tau\bar{\nu}_\tau$  and  $\bar{B} \rightarrow D^{**}\tau\bar{\nu}_\tau$  processes are discussed in section V and VI respectively. Section VII summarizes our results.

## II. THEORETICAL FRAMEWORK

The most general effective Lagrangian of  $b \rightarrow c\tau\bar{\nu}_l$  process can be written as [62]

$$\mathcal{H}_{\text{eff}} = \frac{4G_F}{\sqrt{2}} V_{cb} \left[ (\delta_{l\tau} + V_L) \mathcal{O}_{V_L}^l + V_R \mathcal{O}_{V_R}^l + S_L \mathcal{O}_{S_L}^l + S_R \mathcal{O}_{S_R}^l + T \mathcal{O}_T^l \right], \quad (7)$$

where  $G_F$  is the Fermi constant,  $V_{cb}$  is the CKM matrix element,  $\mathcal{O}_X$ 's ( $X = V_{L,R}, S_{L,R}, T$ ) are the six-dimensional operators

$$\begin{aligned} \mathcal{O}_{V_L}^l &= (\bar{c}_L \gamma^\mu b_L) (\bar{\tau}_L \gamma_\mu \nu_{lL}), & \mathcal{O}_{V_R}^l &= (\bar{c}_R \gamma^\mu b_R) (\bar{\tau}_L \gamma_\mu \nu_{lL}), \\ \mathcal{O}_{S_L}^l &= (\bar{c}_L b_R) (\bar{\tau}_R \nu_{lL}), & \mathcal{O}_{S_R}^l &= (\bar{c}_R b_L) (\bar{\tau}_R \nu_{lL}), \\ \mathcal{O}_T^l &= (\bar{c}_R \sigma^{\mu\nu} b_L) (\bar{\tau}_R \sigma_{\mu\nu} \nu_{lL}), \end{aligned} \quad (8)$$

and the corresponding Wilson coefficients ( $X$ ) are zero in the SM, which can only be generated in NP models. Here  $q_{L(R)} = L(R)q$  are the chiral quark fields with  $L(R) = (1 \mp \gamma_5)/2$  as the projection operators.

Including all the new physics operators, the differential decay rate of  $\bar{B} \rightarrow Pl\bar{\nu}_l$  processes, where  $P = D_{(s)}, \eta_c$  are the pseudo-scalar mesons, with respect to  $q^2$  is given by [62]

$$\begin{aligned} \frac{d\Gamma(\bar{B} \rightarrow Pl\bar{\nu}_l)}{dq^2} &= \frac{G_F^2 |V_{cb}|^2}{192\pi^3 M_B^3} q^2 \sqrt{\lambda_P(q^2)} \left(1 - \frac{m_l^2}{q^2}\right)^2 \\ &\times \left\{ \left|1 + V_L + V_R\right|^2 \left[ \left(1 + \frac{m_l^2}{2q^2}\right) H_0^2 + \frac{3}{2} \frac{m_l^2}{q^2} H_t^2 \right] \right. \\ &+ \frac{3}{2} |S_L + S_R|^2 H_S^2 + 8 |T|^2 \left(1 + \frac{2m_l^2}{q^2}\right) H_T^2 \\ &+ 3 \text{Re} [(1 + V_L + V_R)(S_L^* + S_R^*)] \frac{m_l}{\sqrt{q^2}} H_S H_t \\ &\left. - 12 \text{Re} [(1 + V_L + V_R) T^*] \frac{m_l}{\sqrt{q^2}} H_T H_0 \right\}, \end{aligned} \quad (9)$$

where

$$\lambda_P = \lambda(M_B^2, M_P^2, q^2), \quad \text{with} \quad \lambda(a, b, c) = a^2 + b^2 + c^2 - 2(ab + bc + ca). \quad (10)$$

$M_B$  ( $M_P$ ) is the mass of the  $B$  ( $P$ ) meson,  $m_l$  is the charged lepton mass and  $H_{0,t,S,T}$  are the helicity amplitudes which include the form factors ( $F_{0,1,T}$ ) [62].

The differential decay distribution of  $\bar{B} \rightarrow Vl\bar{\nu}_l$  processes where  $V$  denotes the vector mesons ( $V = D_{(s)}^*, J/\psi$ ), in terms of helicity amplitudes ( $H_{i,\pm}, H_{i,0}, H_t$ , where  $i = V, T$ )

with respect to  $q^2$  is given by [62]

$$\begin{aligned} \frac{d\Gamma(\bar{B} \rightarrow Vl\bar{\nu}_l)}{dq^2} = & \frac{G_F^2 |V_{cb}|^2}{192\pi^3 M_B^3} q^2 \sqrt{\lambda_V(q^2)} \left(1 - \frac{m_l^2}{q^2}\right)^2 \times \\ & \left\{ \left( |1 + V_L|^2 + |V_R|^2 \right) \left[ \left(1 + \frac{m_l^2}{2q^2}\right) (H_{V,+}^2 + H_{V,-}^2 + H_{V,0}^2) + \frac{3}{2} \frac{m_l^2}{q^2} H_{V,t}^2 \right] \right. \\ & - 2\text{Re}[(1 + V_L)V_R^*] \left[ \left(1 + \frac{m_l^2}{2q^2}\right) (H_{V,0}^2 + 2H_{V,+}H_{V,-}) + \frac{3}{2} \frac{m_l^2}{q^2} H_{V,t}^2 \right] \\ & + \frac{3}{2} |S_L - S_R|^2 H_S^2 + 8|T|^2 \left(1 + \frac{2m_l^2}{q^2}\right) (H_{T,+}^2 + H_{T,-}^2 + H_{T,0}^2) \\ & + 3\text{Re}[(1 + V_L - V_R)(S_L^* - S_R^*)] \frac{m_l}{\sqrt{q^2}} H_S H_{V,t} \\ & - 12\text{Re}[(1 + V_L^*)T^*] \frac{m_l}{\sqrt{q^2}} (H_{T,0}H_{V,0} + H_{T,+}H_{V,+} - H_{T,-}H_{V,-}) \\ & \left. + 12\text{Re}[V_R^*T^*] \frac{m_l}{\sqrt{q^2}} (H_{T,0}H_{V,0} + H_{T,+}H_{V,-} - H_{T,-}H_{V,+}) \right\}, \end{aligned} \quad (11)$$

where  $\lambda_V = \lambda(M_B^2, M_V^2, q^2)$ . Alongside the decay rate, we also consider the following angular observables to probe NP in semileptonic  $B$  decays.

**Forward-backward asymmetry :**

$$A_{FB}(q^2) = \left[ \int_{-1}^0 d\cos\theta_l \frac{d^2\Gamma}{dq^2 d\cos\theta_l} - \int_0^1 d\cos\theta_l \frac{d^2\Gamma}{dq^2 d\cos\theta_l} \right]. \quad (12)$$

**Lepton non-universality :**

$$\begin{aligned} R_P &= \frac{\text{Br}(\bar{B} \rightarrow P\tau\bar{\nu})}{\text{Br}(\bar{B} \rightarrow Pl\bar{\nu})}, \\ R_V &= \frac{\text{Br}(\bar{B} \rightarrow V\tau\bar{\nu})}{\text{Br}(\bar{B} \rightarrow Vl\bar{\nu})}, \quad l = e, \mu. \end{aligned} \quad (13)$$

**Tau polarization parameter :**

$$P_\tau(q^2) = \frac{d\Gamma(\lambda_\tau = 1/2)/dq^2 - d\Gamma(\lambda_\tau = -1/2)/dq^2}{d\Gamma(\lambda_\tau = 1/2)/dq^2 + d\Gamma(\lambda_\tau = -1/2)/dq^2}. \quad (14)$$

The detailed expressions for the decay distributions  $d\Gamma(\lambda = \pm 1/2)/dq^2$  can be found in the Ref. [62].

**Polarization of  $V$  :** The longitudinal ( $L$ ) and transverse ( $T$ ) polarization components of daughter vector meson ( $V$ ) are given by [63]

$$F_{L,T}^{D^*}(q^2) = \frac{d\Gamma_{L,T}(\bar{B} \rightarrow D^*\tau\bar{\nu})/dq^2}{d\Gamma(\bar{B} \rightarrow D^*\tau\bar{\nu})/dq^2}. \quad (15)$$

### III. CONSTRAINTS ON NEW COEFFICIENTS

In this section, we perform the  $\chi^2$  fitting to obtain the values of the new coefficients, from the observables  $R_{D^{(*)}}$ ,  $R_{J/\psi}$  and  $\text{Br}(B_c^+ \rightarrow \tau^+ \nu_\tau)$ , where  $\chi^2$  is defined as

$$\chi^2(X) = \sum_i \frac{(\mathcal{O}_i^{\text{th}}(X) - \mathcal{O}_i^{\text{Expt}})^2}{(\Delta \mathcal{O}_i^{\text{Expt}})^2 + (\Delta \mathcal{O}_i^{\text{SM}})^2}. \quad (16)$$

Here  $\mathcal{O}_i^{\text{th}}(X)$  are the total theoretical predictions for the observables with  $X (= V_{L,R}, S_{L,R}, T)$  as the new Wilson coefficients and  $\mathcal{O}_i^{\text{Expt}}$  represent the corresponding measured central values.  $\Delta \mathcal{O}_i^{\text{Expt}}$  and  $\Delta \mathcal{O}_i^{\text{SM}}$  are respectively the experimental and SM uncertainties of the observables. The complete expression for  $\bar{B}(B_c^+) \rightarrow D^{(*)}(J/\psi)l\bar{\nu}_l$  decay rates, required to compute the  $R_{D^{(*)}}$ ,  $R_{J/\psi}$  LNU ratios are provided in the previous section. We use the  $\bar{B} \rightarrow D$  hadronic form factors from [64] that calculated using lattice QCD techniques and for the  $\bar{B} \rightarrow D^*$  decays, we use the heavy quark effective theory (HQET) form factors from [65–67]. For the  $B_c^+ \rightarrow J/\psi$  form factors, we consider the perturbative QCD (PQCD) calculation from [68, 69]. Including the NP contributions, the branching ratios of  $B_c^+ \rightarrow \tau^+ \nu_\tau$  processes is given by [63]

$$\begin{aligned} \text{BR}(B_c^+ \rightarrow \tau^+ \nu_\tau) &= \frac{G_F^2 M_{B_c} m_\tau^2}{8\pi} \left(1 - \frac{m_\tau^2}{M_{B_c}^2}\right)^2 f_{B_c}^2 |V_{cb}|^2 \tau_{B_c^+} \\ &\times \left| (1 + V_L - V_R) - \frac{M_{B_c}^2}{m_\tau(m_b + m_c)} (S_L - S_R) \right|^2. \end{aligned} \quad (17)$$

Using the decay constant,  $f_{B_c} = 489 \pm 4 \pm 3$  MeV from [70, 71] and the CKM matrix elements, particle masses and life time of  $B_c$  meson from [72], the predicted branching fraction in the SM is given as

$$\text{BR}(B_c^+ \rightarrow \tau^+ \nu_\tau)|^{\text{SM}} = (3.6 \pm 0.14) \times 10^{-2}, \quad (18)$$

and its current experimental upper limit is [73]

$$\text{BR}(B_c^+ \rightarrow \tau^+ \nu_\tau)|^{\text{Expt}} < 30\%. \quad (19)$$

In this analysis, we fit all possible cases of new coefficients which are classified as

Case A: Presence of only one new real coefficient at a time.

Case B: Presence of only one new complex coefficient at a time.

Case C: Presence of various combinations of two new real coefficients at a time.

Case A contains individual 5 real new coefficients (vector, scalar and tensor types), whose best-fit values are presented in Table I. In this Table, we have also presented the  $\chi^2_{\text{min, SM+NP}}/\text{d.o.f}$  as well as the pull values, defined as:  $\text{pull} = \sqrt{\chi^2_{\text{SM}} - \chi^2_{\text{SM+NP}}}$ . The degrees of freedom in this case is 3, since we consider four observables with one additional new parameter. We find  $\chi^2_{\text{SM}} = 11.193$  for the SM. The  $\chi^2_{\text{min, SM+V}_L}/\text{d.o.f} = 0.767$  and  $\text{pull} = 2.982$  for the additional  $V_L$  coefficient, which implies the NP contribution due to  $V_L$  coupling, fit the measurement very well. Whereas the presence of  $V_R$ , scalar and tensor type couplings give poor fit to the  $R_{D^{(*)}}$ ,  $R_{J/\psi}$  and  $\text{Br}(B_c^+ \rightarrow \tau^+ \nu_\tau)$  data.

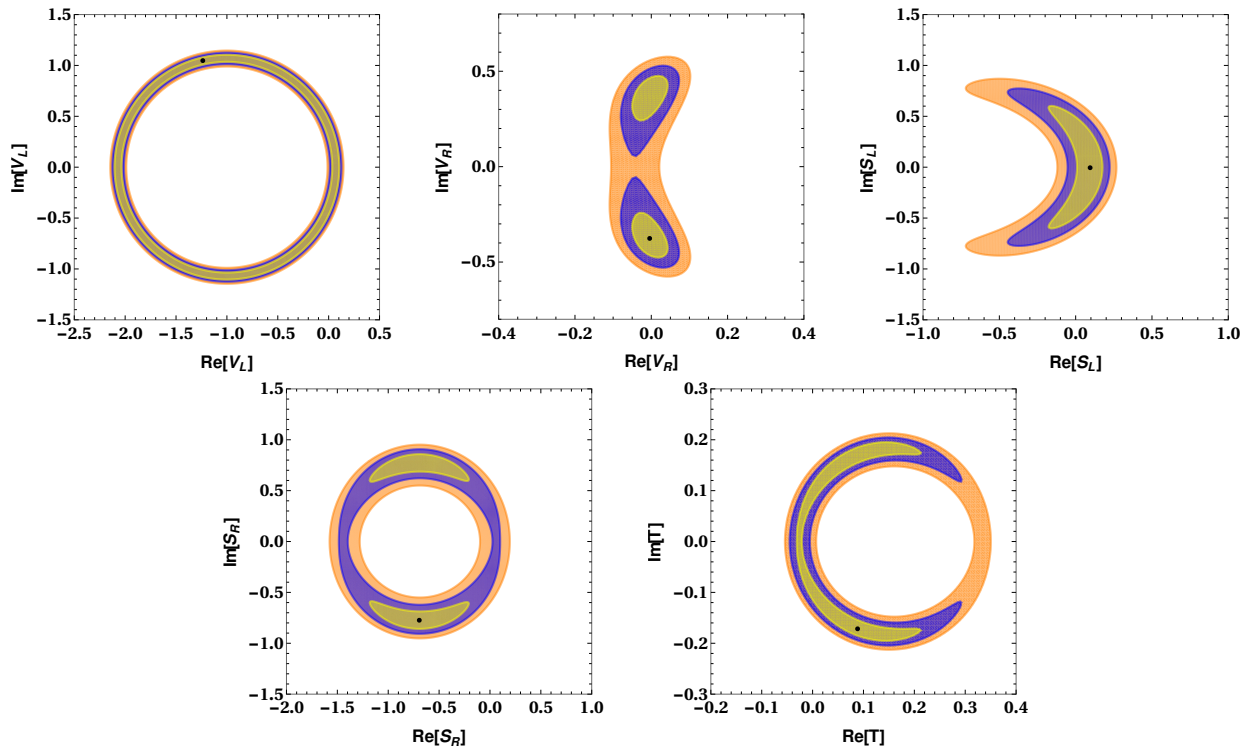


FIG. 1: Constraints on real and imaginary part of the new coefficients obtained from  $\chi^2$  fit to  $R_{D^{(*)}}$ ,  $R_{J/\psi}$  and  $\text{Br}(B_c^+ \rightarrow \tau^+ \nu_\tau)$  observables. Here the black dots represent the best-fit values.

Case B includes the presence of individual complex vector, scalar and tensor type Wilson coefficients. The constrained plots on real and imaginary parts of individual complex Wilson coefficients associated with  $b \rightarrow c\tau\bar{\nu}_\tau$  transitions, obtained from fit to  $R_{D^{(*)}}$ ,  $R_{J/\psi}$  and the upper limit on branching ratio of  $B_c^+ \rightarrow \tau^+ \nu_\tau$  are depicted in Fig. 1. Here yellow, blue and orange colors represent  $1\sigma$ ,  $2\sigma$  and  $3\sigma$  contours respectively and black dots are the respective best-fit values. The pull for only complex  $V_L$  coefficient remain same as previous case and fits the measured data well. We found  $\chi^2_{\text{min, SM+V}_R} = 2.29$  for the complex  $V_R$  coefficient and the pull value has increased from 1.57 to 2.984. The  $S_L$  coefficient fits very poorly with data and the pull remains same as case A. Though their is increment in the pull value of  $S_R$

TABLE I: Predicted best-fit values of new Wilson coefficients for all possible cases. We also provide the  $\chi^2_{\min}/\text{d.o.f}$  and pull values.

Cases	New Wilson coefficients	Best-fit values	$\chi^2_{\min}/\text{d.o.f}$	Pull
Case A	$V_L$	-2.07	0.767	2.982
	$V_R$	-0.0434	2.91	1.57
	$S_L$	0.097	2.81	1.663
	$S_R$	-1.443	3.319	1.112
	$T$	-0.0263	1.6	2.527
Case B	$(\text{Re}[V_L], \text{Im}[V_L])$	(-1.233, 1.045)	1.151	2.982
	$(\text{Re}[V_R], \text{Im}[V_R])$	(-0.0034, -0.3783)	1.145	2.984
	$(\text{Re}[S_L], \text{Im}[S_L])$	(0.97, 0)	4.213	1.663
	$(\text{Re}[S_R], \text{Im}[S_R])$	(-0.695, -0.777)	2.175	2.616
	$(\text{Re}[T], \text{Im}[T])$	(0.0886, -0.17)	1.416	2.892
Case C	$(V_L, V_R)$	(0.0694, -0.0026)	1.147	2.983
	$(V_L, S_L)$	(0.0714, -0.0063)	1.147	2.983
	$(V_L, S_R)$	(0.0724, -0.0086)	1.145	2.984
	$(V_L, T)$	(-0.194, 0.3913)	2.42	2.52
	$(V_R, S_L)$	(-0.09, 0.1726)	1.167	2.976
	$(V_R, S_R)$	(-0.072, 0.154)	1.15	2.96
	$(V_R, T)$	(0.091, -0.0519)	1.02	3.02
	$(S_L, S_R)$	(-1.04, -0.449)	2.72	2.4
	$(S_L, T)$	(-1.25, 0.303)	1.989	2.686
	$(S_R, T)$	(-1.1875, 0.352)	2.23	2.596

and  $T$  coupling as compared to previous case, till they provide poor fit.

Now coming to case C, which includes various possible combination of two real Wilson coefficients at a time. The constrained plots for 10 possible sets of new real coefficients are shown in Fig. 2. We present the zoomed plot for  $V_L - V_R$  coefficients in the top-middle panel of this figure. We find that, the NP contribution arising due to the presence of  $V_L - V_R$ ,  $V_L - S_L$ ,  $V_L - S_R$ ,  $V_R - S_L$  and  $V_R - S_R$  sets of new coefficients provide an acceptable fit with pull values  $\sim 2.96$ . The  $V_R - T$  combination fit the experimental data quite effectively with the highest pull value 3.02. The fit for remaining possible sets of real Wilson coefficients, such as  $V_L \& T$ ,  $S_L \& S_R$ ,  $S_L \& T$ ,  $S_R \& T$  are not robust.

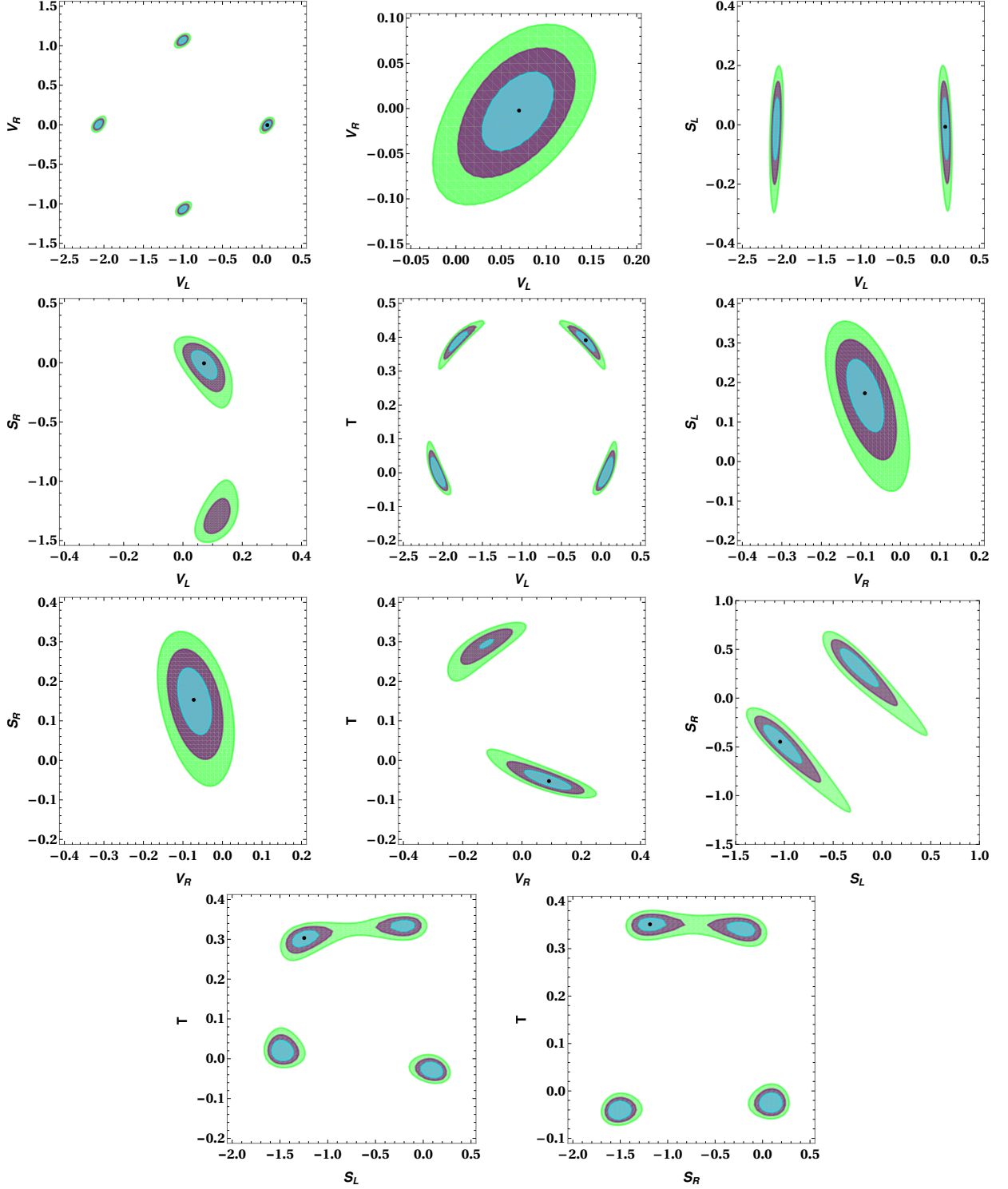


FIG. 2: Constraints on various combination of real new coefficients obtained from  $\chi^2$  fit to  $R_{D^{(*)}}$ ,  $R_{J/\psi}$  and  $\text{Br}(B_c^+ \rightarrow \tau^+ \nu_\tau)$  observables for case C of our analysis. We show the zoom plot for  $V_L - V_R$  plane in the top-middle panel. Here the black dots represent the best-fit values.

## IV. NUMERICAL ANALYSIS FOR $\bar{B} \rightarrow D^{(*)}\tau^-\bar{\nu}_\tau$ , $\bar{B}_s \rightarrow D_s^{(*)}\tau^-\bar{\nu}_\tau$ AND $B_c^+ \rightarrow (\eta_c, J/\psi)\tau^+\nu_\tau$ PROCESSES

After gathering all the information about the constraints on various new coefficients, we now proceed to analyze the impact of NP, for all the possible combinations as discussed above, on branching ratios and various angular observables of  $\bar{B} \rightarrow D^{(*)}\tau^-\bar{\nu}_\tau$ ,  $B_c^+ \rightarrow (\eta_c, J/\psi)\tau^+\nu_\tau$  and  $B_s \rightarrow D_s^{(*)}\tau^-\bar{\nu}_\tau$  decay modes. We study the angular observables of all these decay processes in four  $q^2$  (in  $\text{GeV}^2$ ) bins:  $m_\tau^2 \rightarrow 5$ ,  $5 \rightarrow 7$ ,  $7 \rightarrow 9$  and  $9 \rightarrow (M_B - M_{P(V)})^2$ . All the input parameters required for numerical estimation are taken from [72]. The values of the form factors used in this analysis for various processes are as: (a) lattice QCD results [64] for  $\bar{B} \rightarrow D$  form factors (b) HQET [65–67] results on  $\bar{B} \rightarrow D^*$  form factors (c) the form factors for  $B_c^+ \rightarrow \eta_c$  ( $B_c^+ \rightarrow J/\psi$ ) transitions are from light-front quark model (perturbative QCD) [74] ([68, 69]) (d) lattice QCD results on  $B_s \rightarrow D_s$  form factors [40] and for  $B_s \rightarrow D_s^*$  form factors from perturbative QCD approach [39]. As the tensor form factors for the processes  $B_c^+ \rightarrow (\eta_c, J/\psi)$  and  $B_s \rightarrow D_s^{(*)}$  are not available, we relate them with the respective (axial)vector form factors through the equations of motion. In the following subsections, we discuss our predicted results on all these  $b \rightarrow c\tau\bar{\nu}_\tau$  decay modes for each case.

### A. Case A

Here we consider the presence of a single real new Wilson coefficient at a time, whose predicted best-fit values are presented in Table I. Using these values, the branching ratios of  $\bar{B} \rightarrow D\tau\bar{\nu}_\tau$  (top-left panel),  $\bar{B} \rightarrow D^*\tau\bar{\nu}_\tau$  (top-right panel),  $B_c^+ \rightarrow \eta_c\tau^+\nu_\tau$  (middle-left panel),  $B_c^+ \rightarrow J/\psi\tau^+\nu_\tau$  (middle-right panel),  $B_s \rightarrow D_s\tau\bar{\nu}_\tau$  (bottom-left panel) and  $B_s \rightarrow D_s^*\tau\bar{\nu}_\tau$  (bottom-right panel) processes in four  $q^2$  bins are presented in Fig. 3. The solid red lines in these plots represent the SM predictions and the light red bands represent the SM  $1\sigma$  uncertainties, which arise due to the uncertainties in the input parameters such as CKM matrix elements and hadronic form factors. The dashed blue, green, black, dark yellow and cyan lines are obtained by using the best-fit values of  $V_L$ ,  $V_R$ ,  $S_L$ ,  $S_R$  and  $T$  coefficients, respectively. The following observations are inferred from these plots.

- In  $\bar{B} \rightarrow D$  decays, the  $S_R$  contribution gives significant deviation from the SM in first, second and fourth  $q^2$  bins. The contributions of  $V_L$  and  $S_L$  couplings show reasonable deviations from the SM central values in the second, third and fourth  $q^2$  bins. The predicted branching ratio with  $V_R$  coupling lies within  $1\sigma$  range of SM, while the tensor

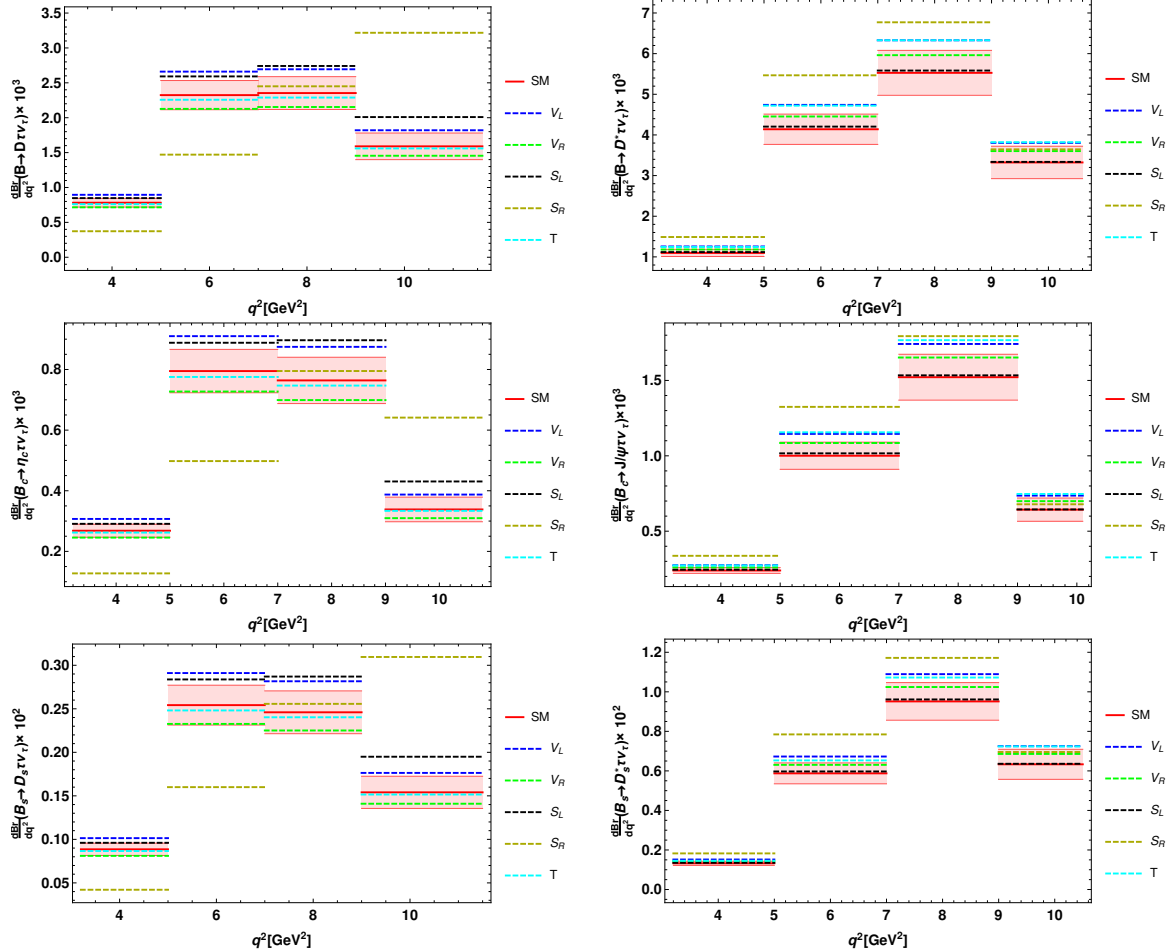


FIG. 3: The bin-wise branching ratios of  $\bar{B} \rightarrow D\tau\bar{\nu}_\tau$  (top-left panel),  $\bar{B} \rightarrow D^*\tau\bar{\nu}_\tau$  (top-right panel),  $B_c^+ \rightarrow \eta_c\tau^+\nu_\tau$  (middle-left panel),  $B_c^+ \rightarrow J/\psi\tau^+\nu_\tau$  (middle-right panel),  $B_s \rightarrow D_s\tau\bar{\nu}_\tau$  (bottom-left panel) and  $B_s \rightarrow D_s^*\tau\bar{\nu}_\tau$  (bottom-right panel) processes in four  $q^2$  bins for case A of our analysis. Here the solid red lines (light red bands) stand for the central values ( $1-\sigma$  uncertainties) in the SM. The blue, green, black, dark yellow and cyan dashed lines are drawn by using the best-fit values of  $V_L$ ,  $V_R$ ,  $S_L$ ,  $S_R$  and  $T$  coefficients, respectively.

coefficient has negligible impact on the entire  $q^2$  region.

- For  $\bar{B} \rightarrow D^*\tau\bar{\nu}_\tau$  process, the branching ratio show significant deviation in the first two bins due to the contribution of additional  $T$  coefficient, whereas the effect of other contributions are rather marginal. The predicted bin-wise branching ratios for  $V_R$  coupling in all bins are found to be within the  $1\sigma$  SM uncertainties. The  $S_L$  coefficient has negligible impact in all four  $q^2$  bins.
- The deviation in the branching fraction of  $B_c^+ \rightarrow \eta_c\tau^+\nu_\tau$  and  $B_s \rightarrow D_s\tau\bar{\nu}_\tau$  processes due to the contribution of  $S_R$  coefficient is significantly large in the first, second and fourth bins whereas the impact of other coefficients are quite marginal in all the bins.

- For  $B_c^+ \rightarrow J/\psi\tau^+\nu_\tau$  ( $B_s \rightarrow D_s^*\tau\bar{\nu}_\tau$ ) process, the effect of  $S_R$  is significantly large in the second (second and third) bin(s), whereas the impact of other couplings are rather nominal.

In order to quantify the above discussed results, we define the pull metric at the observable level as

$$\text{Pull}_i = \frac{\mathcal{O}_i^{\text{NP}} - \mathcal{O}_i^{\text{SM}}}{\sqrt{\Delta\mathcal{O}_i^{\text{NP}}^2 + \Delta\mathcal{O}_i^{\text{SM}}^2}}, \quad (20)$$

where  $i$  represents all observables,  $\mathcal{O}_i^{\text{SM}}$  and  $\mathcal{O}_i^{\text{NP}}$  stand for the values of the observables in the SM and NP scenarios and  $\Delta\mathcal{O}_i^{\text{SM}}$ ,  $\Delta\mathcal{O}_i^{\text{NP}}$  are the corresponding  $1\sigma$  uncertainties. The pull values of the branching fractions of all the decay modes in the presence of individual new coefficients in all the four  $q^2$  bins are presented in Table II. Though the presence of only real  $S_R$  coupling provide comparatively large deviation from the SM results, the corresponding  $\chi^2_{\text{min}}/\text{d.o.f}$  rather large, which implies the fit is not good enough to accommodate all the observed  $b \rightarrow c\tau\bar{\nu}_\tau$  anomalies.

The bin-wise values of forward-backward asymmetry for  $\bar{B} \rightarrow D\tau\bar{\nu}_\tau$  (top-left panel),  $\bar{B} \rightarrow D^*\tau\bar{\nu}_\tau$  (top-right panel),  $B_c^+ \rightarrow \eta_c\tau^+\nu_\tau$  (middle-left panel),  $B_c^+ \rightarrow J/\psi\tau^+\nu_\tau$  (middle-right panel),  $B_s \rightarrow D_s\tau\bar{\nu}_\tau$  (bottom-left panel) and  $B_s \rightarrow D_s^*\tau\bar{\nu}_\tau$  (bottom-right panel) decay modes are represented in Fig. 4. Since the forward-backward asymmetry is independent of  $V_L$  coupling, the presence of only  $V_L$  coefficient does not have any impact on this observable. The forward-backward asymmetry obtained by using the best-fit value of only  $S_R$  coupling has significant deviation from SM results for  $\bar{B} \rightarrow D$ ,  $B_c^+ \rightarrow \eta_c$  and  $B_s \rightarrow D_s$  processes. The remaining coefficients have negligible effect on  $A_{FB}$  of these decay modes. Either  $S_R$  or  $T$  coefficient also provide maximum deviation in all the  $q^2$  bins of  $B_{(s)} \rightarrow D_{(s)}^*$  and  $B_c^+ \rightarrow J/\psi$  processes, except negligible impact of tensor coefficient in the first bin of  $B_c^+ \rightarrow J/\psi$ . The  $V_R$  coefficient also affects this observable, but rather weakly in the last bin.

The graphical representation of lepton non-universality ratios,  $R_D$  (top-left panel),  $R_{D^*}$  (top-right panel),  $R_{\eta_c}$  (middle-left panel),  $R_{J/\psi}$  (middle-right panel),  $R_{D_s}$  (bottom-left panel) and  $R_{D_s^*}$  (bottom-right panel) in four  $q^2$  bins are depicted in Fig. 5. The presence of either  $V_L$ ,  $S_R$  or  $S_L$  coefficients show significant deviation (the  $V_R$  coupling has comparatively less impact) from the SM values of  $R_{D_{(s)}}$  and  $R_{\eta_c}$  observables in the fourth  $q^2$  bin, whereas tensor coupling has vanishingly small effect. All the coefficients except  $S_L$  affect the  $R_{D_{(s)}^*}$  and  $R_{J/\psi}$  observables remarkably in the last three  $q^2$  bins.

The bin-wise plots for the  $\tau$ -polarization asymmetry of  $\bar{B} \rightarrow D\tau\bar{\nu}_\tau$  (top-left panel),  $\bar{B} \rightarrow D^*\tau\bar{\nu}_\tau$  (top-right panel),  $B_c^+ \rightarrow \eta_c\tau^+\nu_\tau$  (middle-left panel),  $B_c^+ \rightarrow J/\psi\tau^+\nu_\tau$  (middle-

TABLE II: Pull values of the branching ratios of all the decay modes in the presence of individual new coefficients in all the four  $q^2$  bins for case A. Here the first row contains the pull values for only  $V_L$ ,  $V_R$ ,  $T$  and second row represents the  $S_L$ ,  $S_R$  pull values.

modes	Only $V_L$	Only $V_R$	Only $T$
	Only $S_L$	Only $S_R$	
$\bar{B} \rightarrow D$	(1.192, 1.06, 0.953, 0.794) (0.72, 0.856, 1.074, 1.364)	(0.783, 0.696, 0.627, 0.522) (5.9, 3.45, 0.285, 3.78)	(0.24, 0.23, 0.197, 0.112)
$\bar{B} \rightarrow D^*$	(1.192, 1.06, 0.953, 0.794) (0.165, 0.123, 0.072, 0.024)	(0.648, 0.574, 0.535, 0.475) (2.65, 2.15, 1.423, 0.544)	(1.1, 1.03, 0.954, 0.82)
$B_c \rightarrow \eta_c$	(1.192, 1.06, 0.953, 0.794) (0.71, 0.87, 1.125, 1.404)	(0.783, 0.696, 0.627, 0.522) (5.925, 3.518, 0.281, 3.482)	(0.206, 0.194, 0.16, 0.082)
$B_c \rightarrow J/\psi$	(1.192, 1.06, 0.953, 0.794) (0.188, 0.124, 0.057, 0.014)	(0.714, 0.635, 0.58, 0.495) (2.95, 2.17, 1.16, 0.318)	(1.143, 1.13, 1.053, 0.88)
$\bar{B} \rightarrow D_s$	(1.192, 1.06, 0.953, 0.794) (0.72, 0.861, 1.09, 1.372)	(0.783, 0.696, 0.625, 0.522) (5.92, 3.485, 0.273, 3.75)	(0.197, 0.191, 0.166, 0.096)
$\bar{B} \rightarrow D_s^*$	(1.192, 1.06, 0.953, 0.794) (0.175, 0.128, 0.074, 0.025)	(0.63, 0.555, 0.52, 0.469) (2.78, 2.234, 1.46, 0.55)	(0.813, 0.829, 0.843, 0.785)

right panel),  $B_s \rightarrow D_s \tau \bar{\nu}_\tau$  (bottom-left panel) and  $B_s \rightarrow D_s^* \tau \bar{\nu}_\tau$  (bottom-right panel) decay modes are shown in Fig. 6. Since the dependence of vector couplings drops out in  $P_\tau$ , so only scalar type couplings provide deviation from SM results for  $B_{(s)} \rightarrow D_{(s)}$  and  $B_c^+ \rightarrow \eta_c$  transitions. We observe that, the contributions from additional  $S_L$  ( $S_R$ ) coefficient affect the  $P_\tau$  observable significantly except in the first (third) bin, whereas tensor coupling has negligible effect in all  $q^2$  bins. In the  $P_\tau^V$  observables ( $V = D_{(s)}^*, J/\psi$ ), the  $S_L$  and  $T$  contributions are dominant in the first two bins and  $S_R$  has significant impact in full  $q^2$  regions. In Fig. 7, the bin-wise plots for longitudinal (left) and transverse (right) polarization asymmetry of  $\bar{B} \rightarrow D^* \tau \bar{\nu}_\tau$ ,  $B_c^+ \rightarrow J/\psi \tau^+ \nu_\tau$  and  $B_s \rightarrow D_s^* \tau \bar{\nu}_\tau$  processes are shown in the top, middle and bottom panels, respectively. Both the longitudinal and transverse polarization asymmetry of all the decay modes shift from their respective SM predictions due to the presence of either  $V_R$  or  $S_R$  couplings. The tensor coefficient affects the first three (two) bins of  $B_c^+ \rightarrow J/\psi$  ( $B_s \rightarrow D_s^*$ ) decay mode.

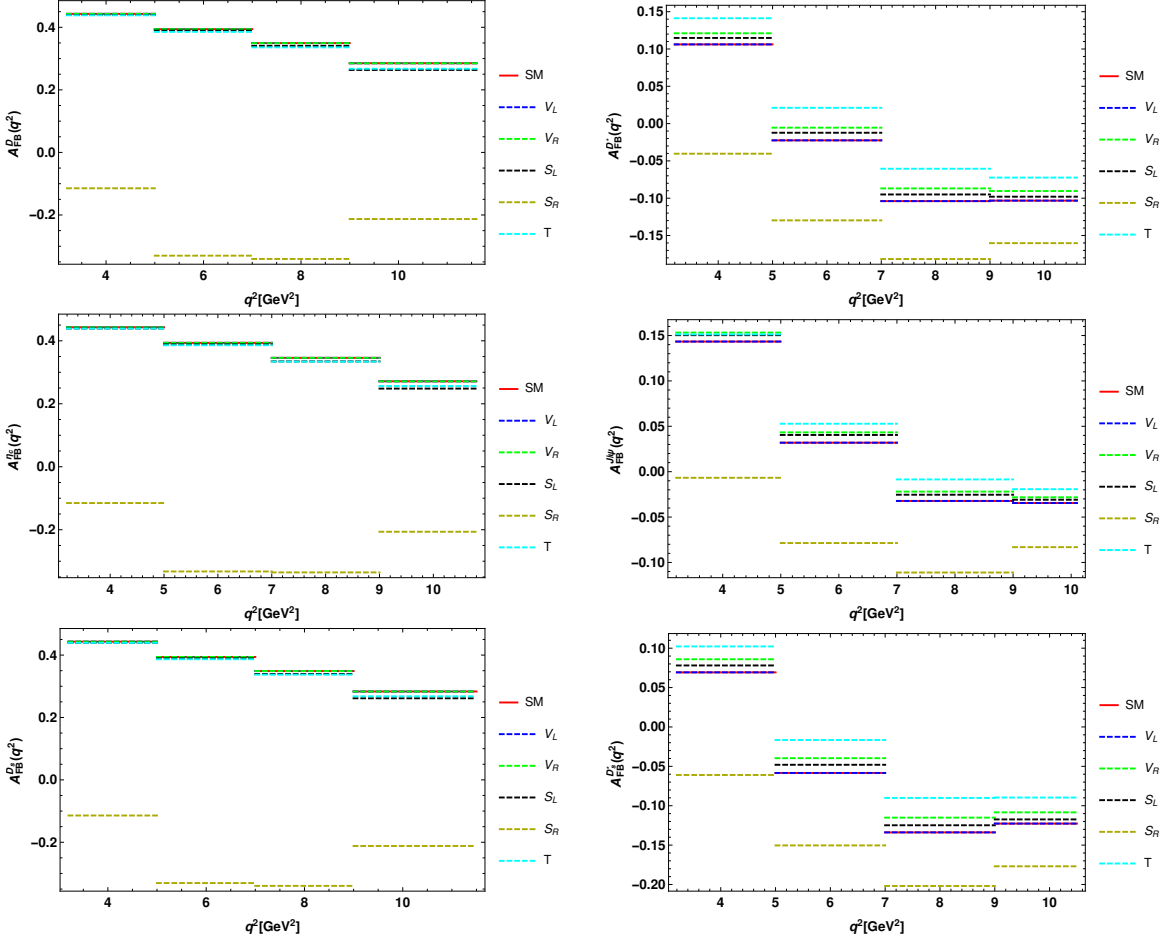


FIG. 4: The bin-wise forward-backward asymmetry of  $\bar{B} \rightarrow D\tau\bar{\nu}_\tau$  (top-left panel),  $\bar{B} \rightarrow D^*\tau\bar{\nu}_\tau$  (top-right panel),  $B_c^+ \rightarrow \eta_c\tau^+\nu_\tau$  (middle-left panel),  $B_c^+ \rightarrow J/\psi\tau^+\nu_\tau$  (middle-right panel),  $B_s \rightarrow D_s\tau\bar{\nu}_\tau$  (bottom-left panel) and  $B_s \rightarrow D_s^*\tau\bar{\nu}_\tau$  (bottom-right panel) processes in four  $q^2$  bins for case A.

## B. Case B

In this case, the new coefficients are assumed to be complex and considering the presence of one coefficient at a time, the best-fit values of the real and imaginary parts of these couplings are presented in Table I. Using the best-fit values, the bin-wise plots for the branching ratio of  $\bar{B} \rightarrow D\tau\bar{\nu}_\tau$  (top-left panel),  $\bar{B} \rightarrow D^*\tau\bar{\nu}_\tau$  (top-right panel),  $B_c^+ \rightarrow \eta_c\tau^+\nu_\tau$  (middle-left panel),  $B_c^+ \rightarrow J/\psi\tau^+\nu_\tau$  (middle-right panel),  $B_s \rightarrow D_s\tau\bar{\nu}_\tau$  (bottom-left panel) and  $B_s \rightarrow D_s^*\tau\bar{\nu}_\tau$  (bottom-right panel) decay processes are shown in Fig. 8. In the presence of either  $V_L$  or  $V_R$  coefficient, the branching ratios of all the decay modes deviate from their SM values in all the bins except the first bin (where the deviation is minimal). Due to the additional  $S_L$  coupling, the branching fractions of  $B_{(s)} \rightarrow D_{(s)}$  and  $B_c^+ \rightarrow \eta_c$  show significant deviations in all bins except in the first one, whereas  $B_{(s)} \rightarrow D_{(s)}^*$  and  $B_c^+ \rightarrow J/\psi$

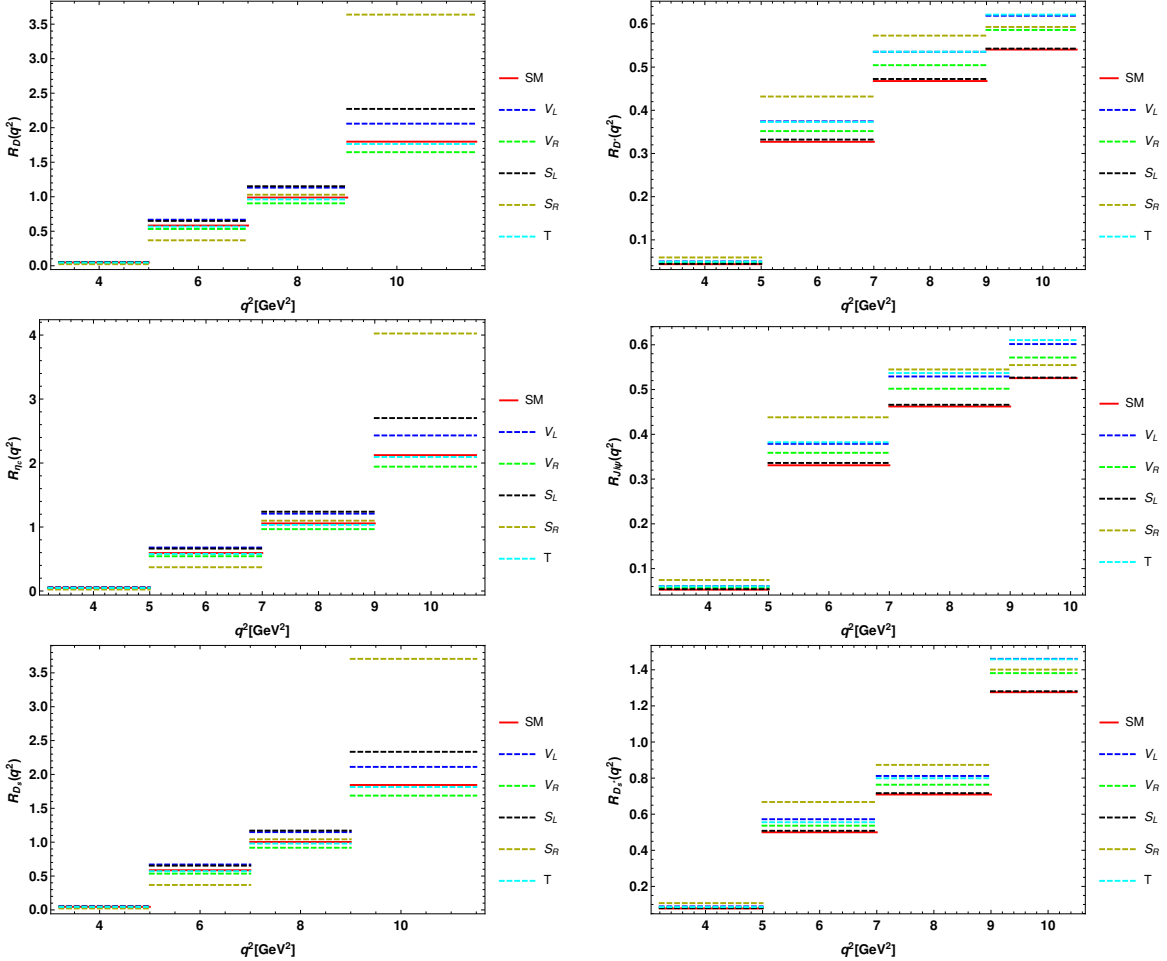


FIG. 5: The bin-wise  $R_D$  (top-left panel),  $R_{D^*}$  (top-right panel),  $R_{\eta_c}$  (middle-left panel),  $R_{J/\psi}$  (middle-right panel),  $R_{D_s}$  (bottom-left panel) and  $R_{D_s^*}$  (bottom-right panel) in four  $q^2$  bins for case A.

have negligibly effect from  $S_L$ . The branching ratios of all processes deviate maximally due to the new contribution from  $S_R$  coefficient. The tensor coefficient affects 2<sup>nd</sup> and 3<sup>rd</sup> bins of  $B_{(s)} \rightarrow D_{(s)}$  and  $B_c^+ \rightarrow \eta_c$ , first three bins of  $B_{(s)} \rightarrow D_{(s)}^*$  and no effect on  $B_c^+ \rightarrow J/\psi$ . For this case, the pull values of the branching ratios of all these channels in the presence of individual complex coefficient, in all the four  $q^2$  bins are given in Table III.

The graphical representation of forward-backward asymmetry of  $\bar{B} \rightarrow D\tau\bar{\nu}_\tau$  (top-left panel),  $\bar{B} \rightarrow D^*\tau\bar{\nu}_\tau$  (top-right panel),  $B_c^+ \rightarrow \eta_c\tau^+\nu_\tau$  (middle-left panel),  $B_c^+ \rightarrow J/\psi\tau^+\nu_\tau$  (middle-right panel),  $B_s \rightarrow D_s\tau\bar{\nu}_\tau$  (bottom-left panel) and  $B_s \rightarrow D_s^*\tau\bar{\nu}_\tau$  (bottom-right panel) decay processes are shown in Fig. 9. The presence of  $V_R$  coefficient affects the forward-backward asymmetry of only  $B \rightarrow V$  processes. The  $S_L$  coupling shows vanishing results. The  $S_R$  coefficients contributes maximally to the forward-backward asymmetry of all these decay modes in all the four  $q^2$  bin. The tensor coefficients show deviation in the last three bins of  $B_{(s)} \rightarrow D_{(s)}$  ( $B_c^+ \rightarrow \eta_c$ ), first three bins of  $B_{(s)} \rightarrow D_{(s)}^*$  and first two bins of

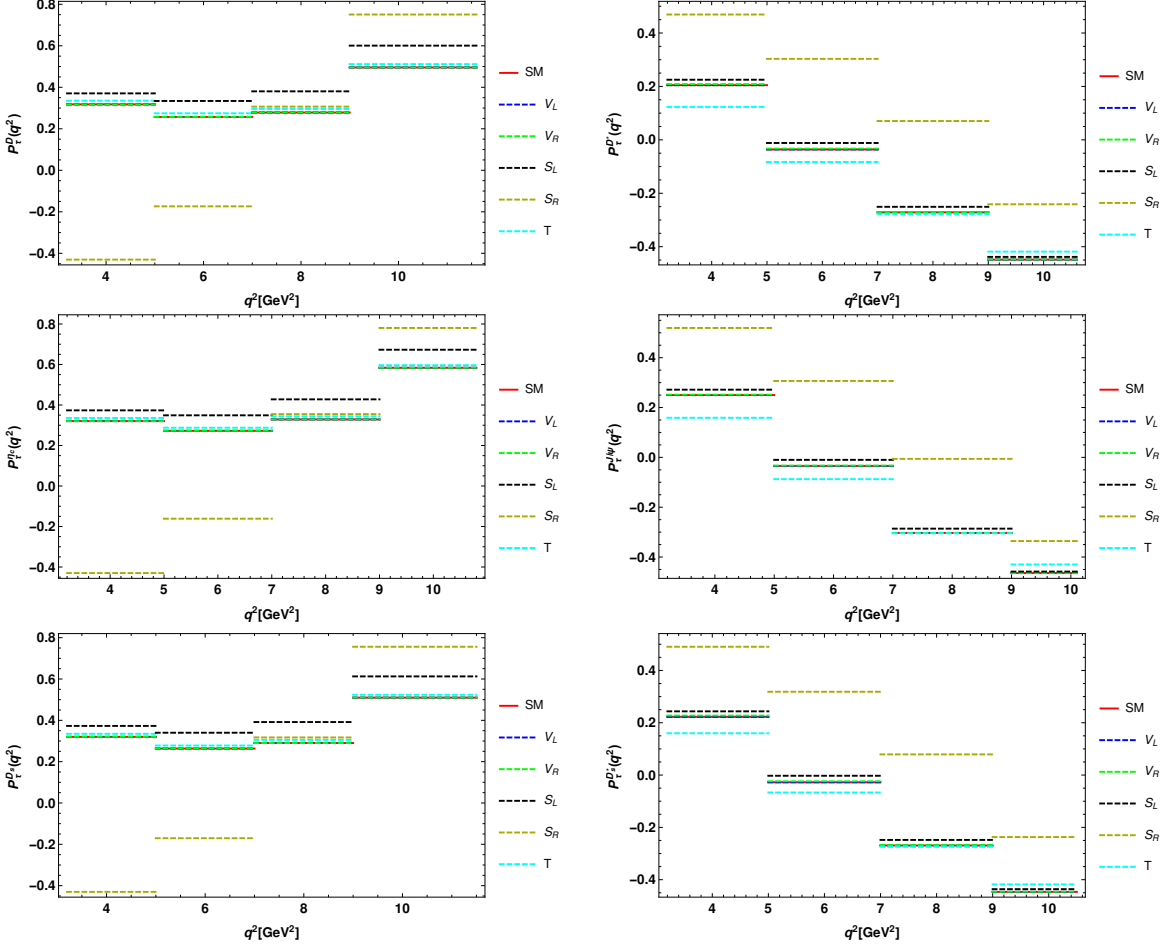


FIG. 6: The bin-wise  $\tau$ -polarization asymmetry of  $\bar{B} \rightarrow D\tau\bar{\nu}_\tau$  (top-left panel),  $\bar{B} \rightarrow D^*\tau\bar{\nu}_\tau$  (top-right panel),  $B_c^+ \rightarrow \eta_c\tau^+\nu_\tau$  (middle-left panel),  $B_c^+ \rightarrow J/\psi\tau^+\nu_\tau$  (middle-right panel),  $\bar{B}_s \rightarrow \bar{D}_s\tau\bar{\nu}_\tau$  (bottom-left panel) and  $\bar{B}_s \rightarrow \bar{D}_s^*\tau\bar{\nu}_\tau$  (bottom-right panel) processes in four  $q^2$  bins for case A.

$B_c^+ \rightarrow J/\psi$  process. The bin-wise numerical values of branching ratios and forward-backward asymmetries are given in Table IV .

The bin-wise values of  $R_D$  (top-left panel),  $R_{D^*}$  (top-right panel),  $R_{\eta_c}$  (middle-left panel),  $R_{J/\psi}$  (middle-right panel),  $R_{D_s}$  (bottom-left panel) and  $R_{D_s^*}$  (bottom-right panel) are presented graphically in Fig. 10 . All the coefficients provide profound deviations in the last  $q^2$  bin of  $R_{D(s)}$  and  $R_{\eta_c}$  observables. Including either  $V_L$  or  $V_R$  coefficient, we find significant deviation in the last three bins of the  $R_V$  observable and the additional  $S_R$  coupling maximally affect the two middle bins. The  $S_L$  coefficient has negligible impact on these LNU parameters, whereas tensor coupling affects the second and third bins of  $R_{D_s^*}$ . Though  $T$  coupling has impact on last bin of  $B_c^+ \rightarrow J/\psi$ , the deviation is minimal.

The graphical representation of tau polarization observable of  $\bar{B} \rightarrow D\tau\bar{\nu}_\tau$  (top-left panel),  $\bar{B} \rightarrow D^*\tau\bar{\nu}_\tau$  (top-right panel),  $B_c^+ \rightarrow \eta_c\tau^+\nu_\tau$  (middle-left panel),  $B_c^+ \rightarrow J/\psi\tau^+\nu_\tau$  (middle-right panel),  $B_s \rightarrow D_s\tau\bar{\nu}_\tau$  (bottom-left panel) and  $B_s \rightarrow D_s^*\tau\bar{\nu}_\tau$  (bottom-right panel) decay

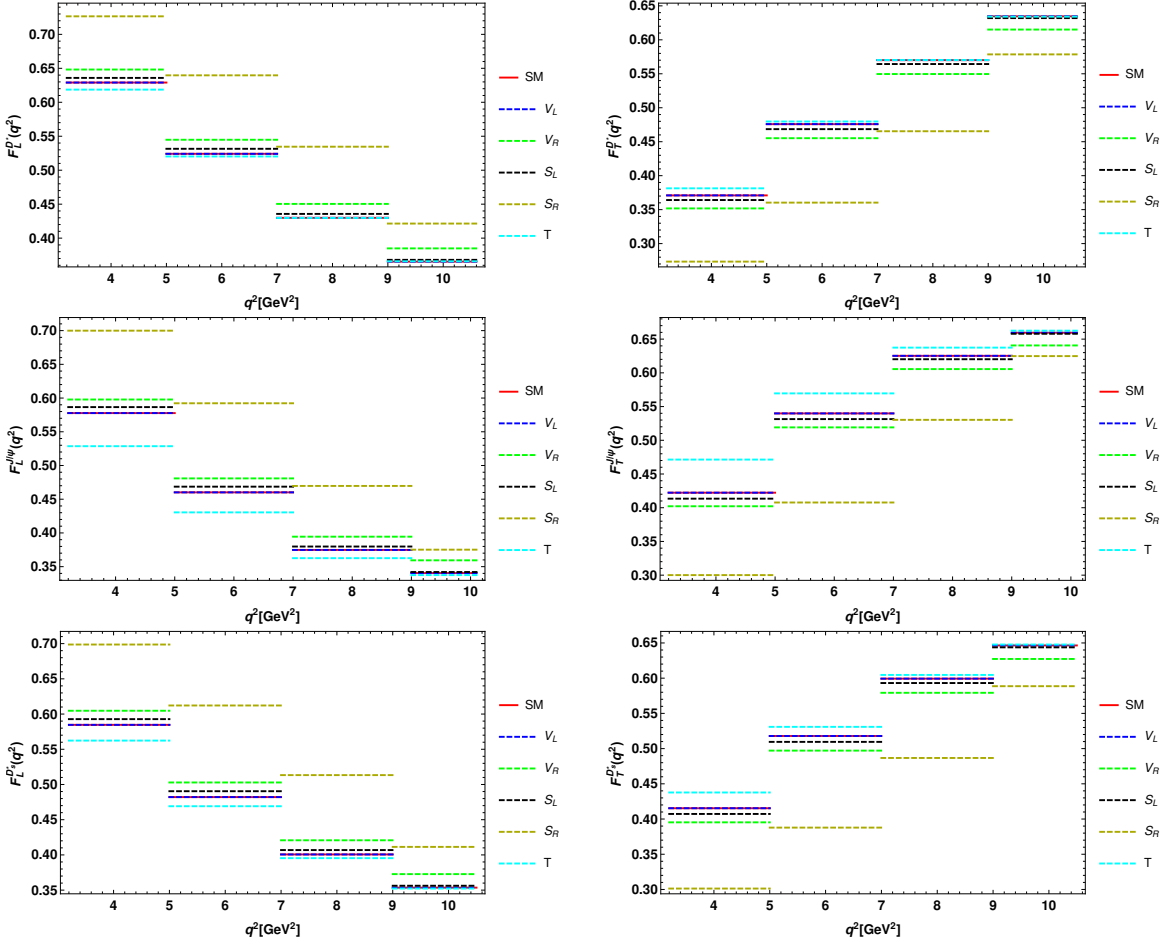


FIG. 7: The bin-wise longitudinal (left panel) and transverse (right panel) polarization asymmetry of daughter vector meson of  $\bar{B} \rightarrow D^* \tau \bar{\nu}_\tau$  (top),  $B_c^+ \rightarrow J/\psi \tau^+ \nu_\tau$  (middle) and  $B_s \rightarrow D_s^* \tau \bar{\nu}_\tau$  (bottom) processes in four  $q^2$  bins for case A.

processes are shown in Fig. 11. The  $S_L$  coefficient has significant impact on  $P_\tau$  observable of  $B \rightarrow P$  and almost null effect on  $B \rightarrow V$  decay modes. The inclusion of either  $S_R$  or  $T$  coefficient has shifted  $P_\tau$  significantly from the SM values of all decay modes. The bin-wise numerical values of the LNU ratios and  $\tau$  polarization asymmetries are presented in Table V.

Fig. 12 depicts the bin-wise plots for longitudinal (left) and transverse (right) polarization asymmetry parameters of  $\bar{B} \rightarrow D^* \tau \bar{\nu}_\tau$  (top),  $B_c^+ \rightarrow J/\psi \tau^+ \nu_\tau$  (middle) and  $B_s \rightarrow D_s^* \tau \bar{\nu}_\tau$  (bottom) processes for case B. The  $F_L$  and  $F_T$  parameters of none of the decay modes are affected by the  $V_L/V_R/S_L$  coefficients, whereas  $S_R/T$  have significant impact on the decay modes in all the  $q^2$  bins. The bin-wise numerical values of longitudinal polarization asymmetries of  $D_{(s)}^*$ ,  $J/\psi$  vector mesons are presented in Table VI. The transverse polarization asymmetries can be obtained from Table VI by using the relation  $F_T = 1 - F_L$ . Fig. 19 depicts the correlations between lepton non-universality, lepton and hadron longitudinal po-

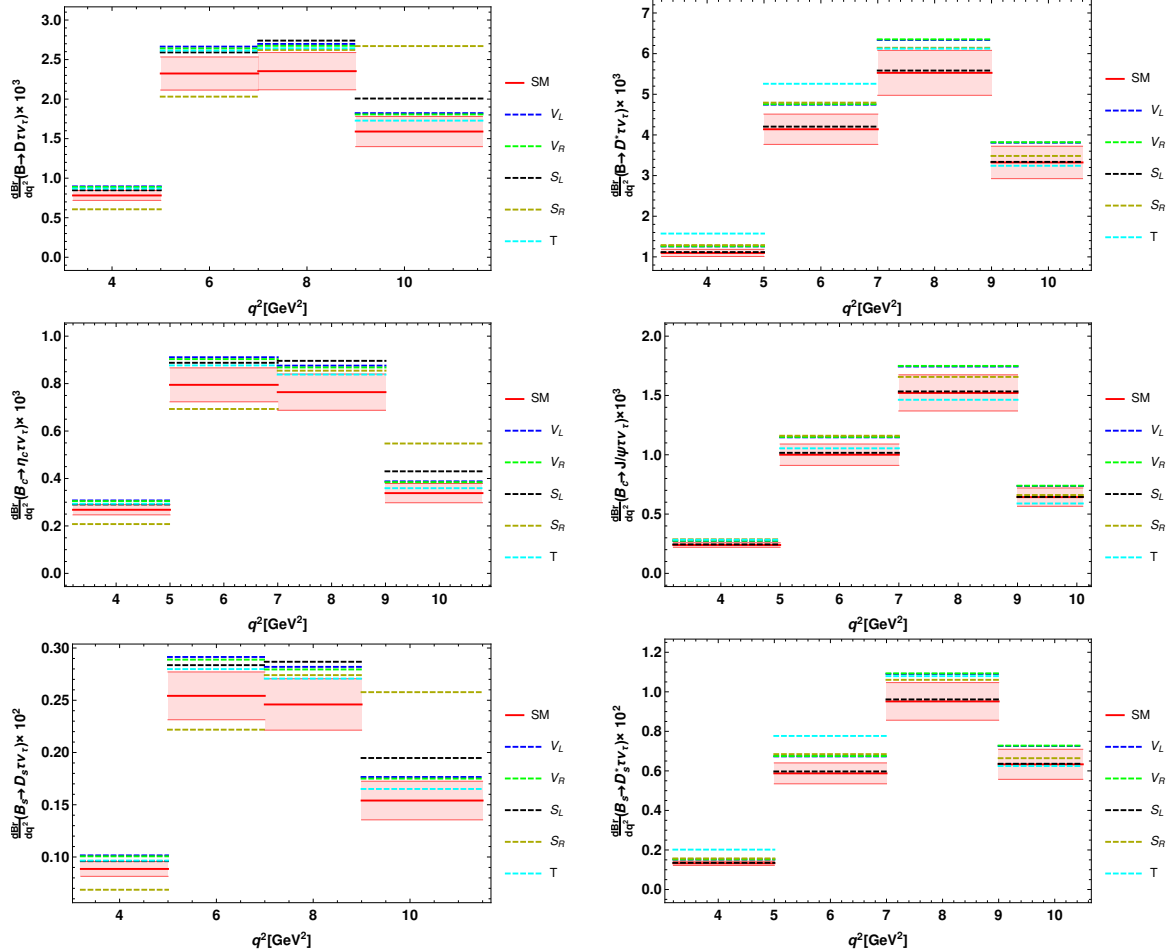


FIG. 8: The bin-wise branching ratios of  $\bar{B} \rightarrow D\tau\bar{\nu}_\tau$  (top-left panel),  $\bar{B} \rightarrow D^*\tau\bar{\nu}_\tau$  (top-right panel),  $B_c^+ \rightarrow \eta_c\tau^+\nu_\tau$  (middle-left panel),  $B_c^+ \rightarrow J/\psi\tau^+\nu_\tau$  (middle-right panel),  $\bar{B}_s \rightarrow \bar{D}_s\tau\bar{\nu}_\tau$  (bottom-left panel) and  $\bar{B}_s \rightarrow \bar{D}_s^*\tau\bar{\nu}_\tau$  (bottom-right panel) processes in four  $q^2$  bins for case B.

larization asymmetries of all the above discussed decay modes in their corresponding full  $q^2$  range that obtained by using the  $1\sigma$  range of new coefficients for case B. The  $1\sigma$  range of new vector and scalar complex coefficients obtained from the joint confidence regions of the real and imaginary planes of these new couplings are given in Table III of our previous work [75]. The  $1\sigma$  ranges of real and imaginary parts of the tensor coefficient are  $(\text{Re}[T], \text{Im}[T]) = ([0.066, 0.12], [-0.18, -0.16])$ .

### C. Case C

In this subsection, we discuss the implications of two different types of real Wilson coefficients on the branching fractions, LNU ratios and angular observables of  $B_{(s)} \rightarrow D_{(s)}^{(*)}\tau\bar{\nu}_\tau$  and  $B_c^+ \rightarrow (\eta_c, J/\psi)\tau^+\nu_\tau$  decay processes. We consider 10 possible combinations of new coefficients such as  $(V_L, V_R)$ ,  $(V_L, S_L)$ ,  $(V_L, S_R)$ ,  $(V_L, T)$ ,  $(V_R, S_L)$ ,  $(V_R, S_R)$ ,  $(V_R, T)$ ,  $(S_L, S_R)$ ,

TABLE III: Pull values of the branching ratios of all the decay modes in the presence of individual new coefficients in all the four  $q^2$  bins for case B. Here the first row contains the pull values for only  $V_L$ ,  $V_R$ ,  $T$  and second row represents the  $S_L$ ,  $S_R$  pull values.

modes	Only $V_L$	Only $V_R$	Only $T$
	Only $S_L$	Only $S_R$	
$\bar{B} \rightarrow D$	(1.2, 1.07, 0.962, 0.802) (0.712, 0.853, 1.07, 1.36)	(1.13, 1.0, 0.9, 0.751) (2.215, 1.053, 0.762, 2.9)	(0.942, 0.921, 0.818, 0.49)
$\bar{B} \rightarrow D^*$	(1.2, 1.07, 0.962, 0.802) (0.164, 0.122, 0.072, 0.242)	(1.23, 1.086, 0.979, 0.818) (1.42, 1.149, 0.746, 0.277)	(3.102, 1.86, 0.722, 0.147)
$B_c \rightarrow \eta_c$	(1.2, 1.07, 0.962, 0.802) (0.715, 0.867, 1.121, 1.4)	(1.13, 1.0, 0.9, 0.751) (2.23, 1.07, 0.79, 2.71)	(0.797, 0.797, 0.655, 0.35)
$B_c \rightarrow J/\psi$	(1.2, 1.07, 0.962, 0.802) (0.187, 0.123, 0.057, 0.014)	(1.23, 1.1, 0.983, 0.82) (1.6, 1.16, 0.6, 0.16)	(1.48, 0.41, 0.274, 0.512)
$\bar{B} \rightarrow D_s$	(1.2, 1.07, 0.962, 0.802) (0.713, 0.857, 1.08, 1.37)	(1.13, 1.0, 0.9, 0.751) (2.23, 1.07, 0.763, 2.879)	(0.762, 0.753, 0.677, 0.41)
$\bar{B} \rightarrow D_s^*$	(1.2, 1.07, 0.962, 0.802) (0.174, 0.127, 0.074, 0.025)	(1.22, 1.085, 0.978, 0.818) (1.5, 1.197, 0.766, 0.281)	(3.587, 2.16, 0.89, 0.082)

$(S_L, T)$  and  $(S_R, T)$ , whose best-fit values are presented in Table I. Using the best-fit values, the branching ratios of  $\bar{B} \rightarrow D\tau\bar{\nu}_\tau$  (top-left panel),  $\bar{B} \rightarrow D^*\tau\bar{\nu}_\tau$  (top-right panel),  $B_c^+ \rightarrow \eta_c\tau^+\nu_\tau$  (middle-left panel),  $B_c^+ \rightarrow J/\psi\tau^+\nu_\tau$  (middle-right panel),  $B_s \rightarrow D_s\tau\bar{\nu}_\tau$  (bottom-left panel) and  $B_s \rightarrow D_s^*\tau\bar{\nu}_\tau$  (bottom-right panel) processes in four  $q^2$  bin for all possible set of coefficients are presented in Fig. 13. Here blue, green, magenta, dark yellow represents the  $V_L \& V_R$ ,  $V_L \& S_L$ ,  $V_L \& S_R$ ,  $V_L \& T$  sets respectively. The orange, purple, black colors are respectively stand for  $V_R \& S_L$ ,  $V_R \& S_R$ ,  $V_R \& T$  and cyan, dark green, gray are for  $S_L \& S_R$ ,  $S_L \& T$ ,  $S_R \& T$  combinations, respectively. In the first bin of  $\text{Br}(\bar{B} \rightarrow D\tau\bar{\nu}_\tau)$ , the  $V_R \& S_L$ ,  $V_R \& S_R$  and  $S_R \& T$  have negligible deviation, slight deviation has been found for the sets  $V_L \& V_R$ ,  $V_L \& S_L$ ,  $V_L \& S_R$ ,  $V_L \& T$ ,  $V_R \& T$  and  $S_L \& T$  and significant deviation from the SM predictions are noticed for the  $S_L \& S_R$  combination of Wilson coefficients. The  $V_R \& S_L$  and  $V_R \& S_R$  provide no deviation, whereas  $V_L \& V_R$ ,  $V_L \& S_L$ ,  $V_L \& S_R$ ,  $V_L \& T$  and  $S_L \& S_R$  give significant deviations from the SM results in the second bin and the  $S_L \& S_R$  show maximum deviation. In the 3<sup>rd</sup> bin, all combinations of real coefficients provide significant contribu-

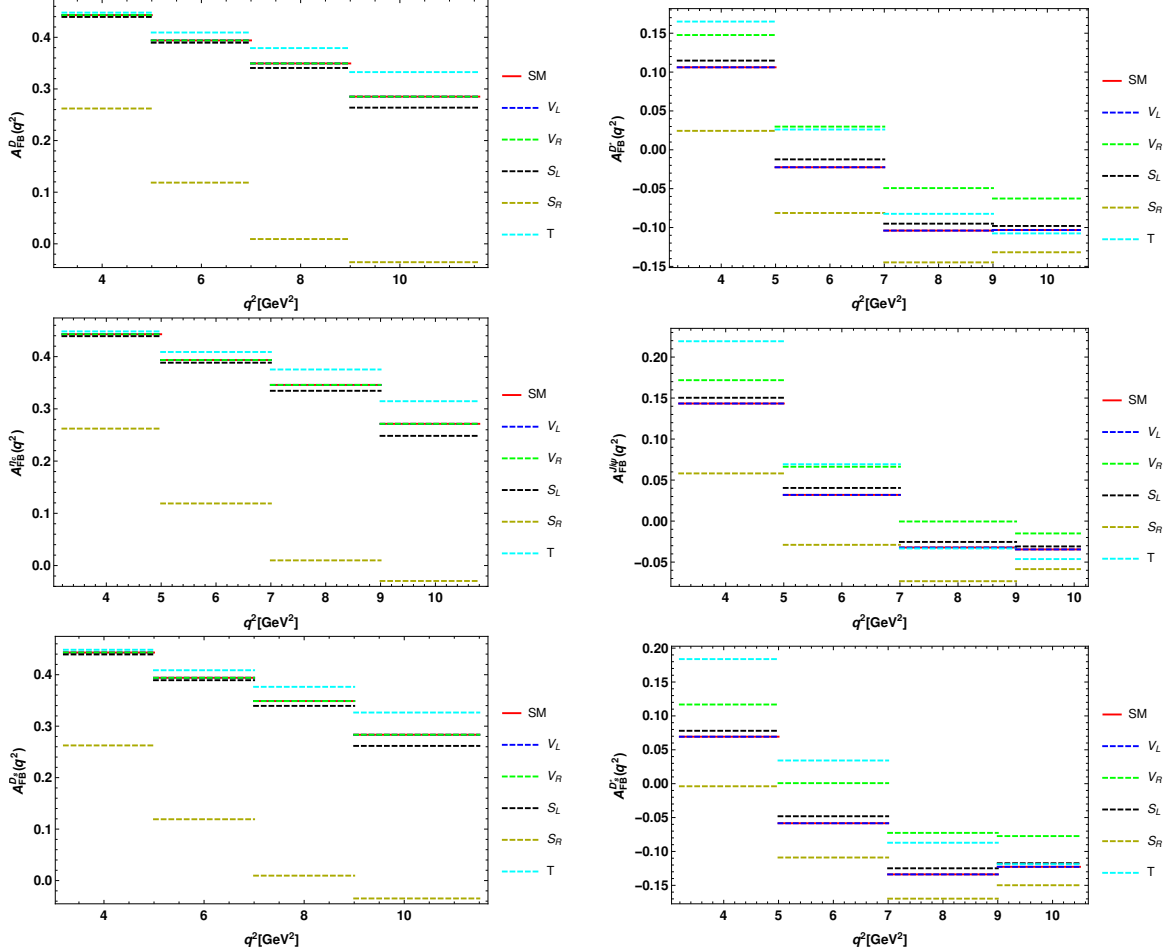


FIG. 9: The bin-wise forward-backward asymmetry of  $\bar{B} \rightarrow D\tau\bar{\nu}_\tau$  (top-left panel),  $\bar{B} \rightarrow D^*\tau\bar{\nu}_\tau$  (top-right panel),  $B_c^+ \rightarrow \eta_c\tau^+\nu_\tau$  (middle-left panel),  $B_c^+ \rightarrow J/\psi\tau^+\nu_\tau$  (middle-right panel),  $\bar{B}_s \rightarrow \bar{D}_s\tau\bar{\nu}_\tau$  (bottom-left panel) and  $\bar{B}_s \rightarrow \bar{D}_s^*\tau\bar{\nu}_\tau$  (bottom-right panel) processes in four  $q^2$  bins for case B.

tions. Except  $V_L \& T$ , all the sets of Wilson coefficients provide large deviation in the last  $q^2$  bin. The branching ratio of  $\bar{B} \rightarrow D^*\tau\bar{\nu}_\tau$  is found to receive significant new physics contribution from all possible combinations of coefficients except  $S_L \& S_R$  in all the  $q^2$  bins. The  $V_R \& T$ ,  $S_L \& S_R$ ,  $S_L \& T$  and  $S_R \& T$  sets provide deviation (deviation is maximum for  $S_L \& S_R$ ) in the first two bins of the branching ratios of  $B_c \rightarrow \eta_c\tau\bar{\nu}_l$ . Except  $V_L \& T$ ,  $S_L \& T$  and  $S_R \& T$ , the  $\text{Br}(B_c \rightarrow \eta_c)$  in 3<sup>rd</sup> bin deviate significantly due to the presence of rest combinations of Wilson coefficients. All the sets show significant deviation in the last bin and the maximum deviation is observed for the  $S_L \& S_R$  set. The bin-wise predictions on the branching ratio of  $B_s \rightarrow D_s\tau\bar{\nu}_\tau$  behave almost similarly as  $\bar{B} \rightarrow \bar{D}$ .

In Fig. 14, we show the bin-wise forward-backward asymmetry values of  $\bar{B} \rightarrow D\tau\bar{\nu}_\tau$  (top-left panel),  $\bar{B} \rightarrow D^*\tau\bar{\nu}_\tau$  (top-right panel),  $B_c^+ \rightarrow \eta_c\tau^+\nu_\tau$  (middle-left panel),  $B_c^+ \rightarrow J/\psi\tau^+\nu_\tau$  (middle-right panel),  $B_s \rightarrow D_s\tau\bar{\nu}_\tau$  (bottom-left panel) and  $B_s \rightarrow D_s^*\tau\bar{\nu}_\tau$  (bottom-right panel)

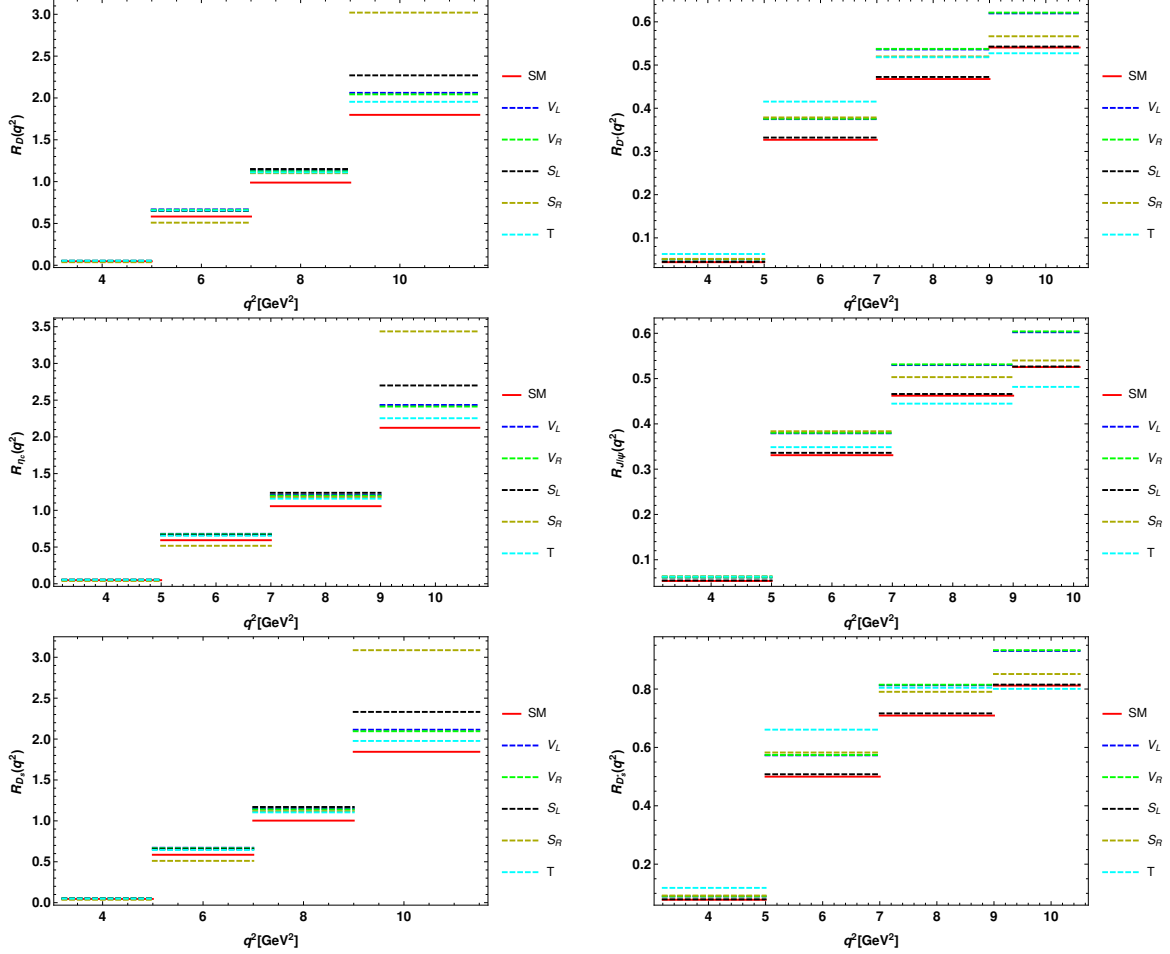


FIG. 10: The bin-wise  $R_D$  (top-left panel),  $R_{D^*}$  (top-right panel),  $R_{\eta_c}$  (middle-left panel),  $R_{J/\psi}$  (middle-right panel),  $R_{D_s}$  (bottom-left panel) and  $R_{D_s^*}$  (bottom-right panel) in four  $q^2$  bins for case B.

processes. We observe that the  $S_L \& S_R$ ,  $S_L \& T$  and  $S_R \& T$  coefficients provide significant deviation from the SM predictions of forward-backward asymmetry of  $B_{(s)} \rightarrow D_{(s)}$  and  $B_c^+ \rightarrow \eta_c$  in all  $q^2$  bins, however  $V_L \& T$  affect the  $A_{FB}$  parameter in the last bins. Except the  $V_L \& V_R$ ,  $V_L \& S_L$  and  $V_L \& S_R$ , all possible coefficients combinations shift the  $A_{FB}$  of  $B_{(s)} \rightarrow D_{(s)}^*$  and  $B_c^+ \rightarrow J/\psi$  decay modes. The  $S_L \& T$  set has no effect on the forward-backward asymmetry of  $\bar{B} \rightarrow D^*$  in the third bin.

Fig. 15 depicts the bin-wise values of lepton non-universality observables of  $\bar{B} \rightarrow D\tau\bar{\nu}_\tau$  (top-left panel),  $\bar{B} \rightarrow D^*\tau\bar{\nu}_\tau$  (top-right panel),  $B_c^+ \rightarrow \eta_c\tau^+\nu_\tau$  (middle-left panel),  $B_c^+ \rightarrow J/\psi\tau^+\nu_\tau$  (middle-right panel),  $B_s \rightarrow D_s\tau\bar{\nu}_\tau$  (bottom-left panel) and  $B_s \rightarrow D_s^*\tau\bar{\nu}_\tau$  (bottom-right panel) decay modes. All the sets of combinations have significant effects on the  $R_{D_{(s)}}$ ,  $R_{\eta_c}$  parameters in the last  $q^2$  bin except  $V_L \& T$ , which provides negligible deviation. The  $V_L \& T$  and  $S_R \& T$  coefficients deviates significantly from SM results of  $R_{D_{(s)}}$  ( $R_{J/\psi}$ ) in the last three (two) bins. The  $S_L \& T$  coefficient show maximum deviation in  $R_V$  ratios.

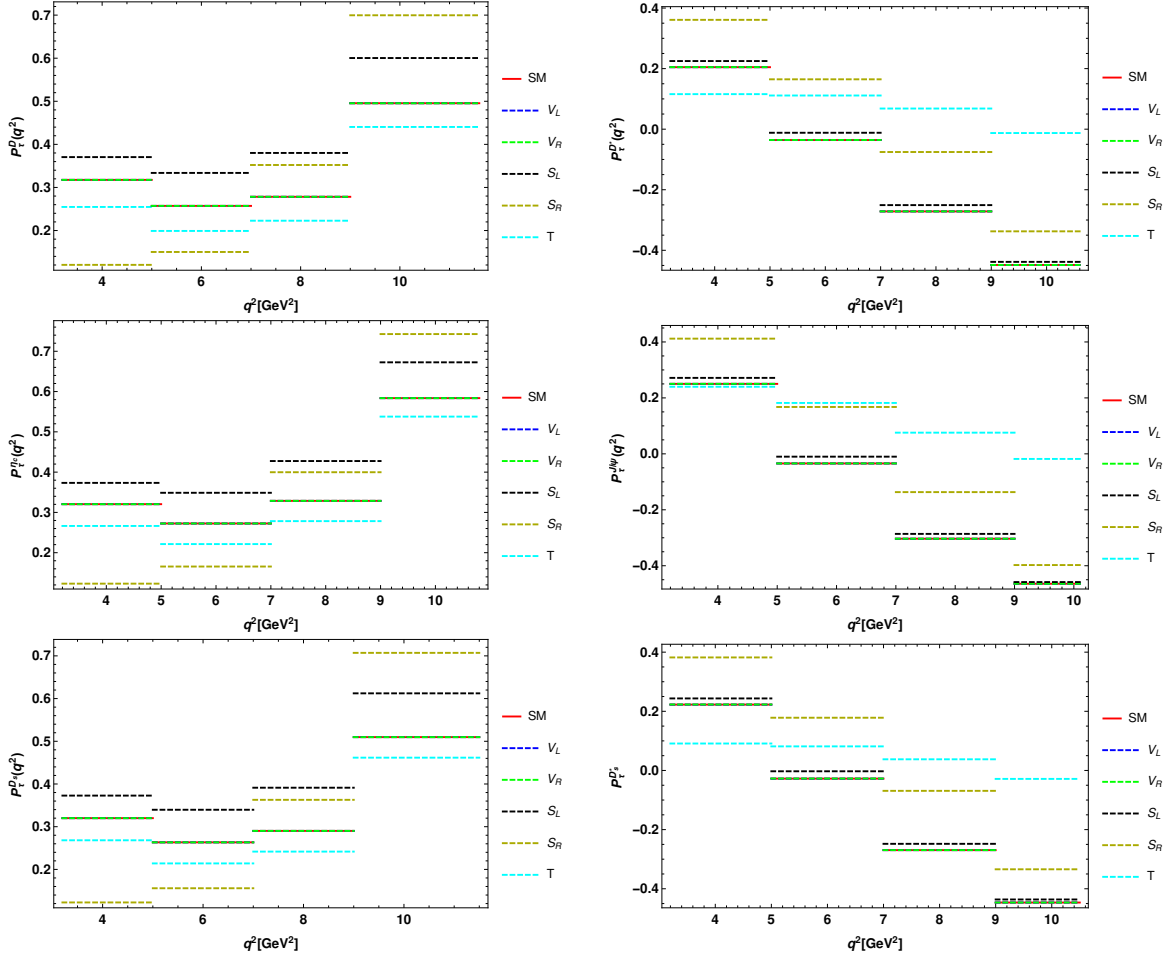


FIG. 11: The bin-wise  $\tau$ -polarization asymmetry of  $\bar{B} \rightarrow D\tau\bar{\nu}_\tau$  (top-left panel),  $\bar{B} \rightarrow \bar{D}^*\tau\nu_\tau$  (top-right panel),  $B_c^+ \rightarrow \eta_c\tau^+\nu_\tau$  (middle-left panel),  $B_c^+ \rightarrow J/\psi\tau^+\nu_\tau$  (middle-right panel),  $\bar{B}_s \rightarrow \bar{D}_s\tau\bar{\nu}_\tau$  (bottom-left panel) and  $\bar{B}_s \rightarrow \bar{D}_s^*\tau\bar{\nu}_\tau$  (bottom-right panel) processes in four  $q^2$  bins for case B.

The graphical representation of tau polarization asymmetry of all these decay modes are presented in Fig. 16. For all  $B \rightarrow P$  decay modes, the  $V_L \& V_R$ ,  $V_L \& S_L$  and  $V_L \& S_R$  scenario provide no deviation from the SM predictions in all the  $q^2$  bins and the  $S_L \& T$  set has negligible effect on the 1<sup>st</sup> bin of  $P_\tau^{D(s)}$ . The impact of  $S_{L(R)} \& T$  and  $V_L \& T$  scenarios on  $\tau$ -polarization asymmetries of  $B \rightarrow V$  processes are far-reaching. Similarly, all possible combinations of Wilson coefficients have larger impact on  $V$  polarization asymmetries of  $B \rightarrow V$ , except the  $V_L \& V_R$ ,  $V_L \& S_L$  and  $V_L \& S_R$  scenarios.

#### V. $\Lambda_b \rightarrow \Lambda_c\tau\bar{\nu}_\tau$

This section discusses the decay rates and angular observables of  $\Lambda_b \rightarrow \Lambda_c\tau\bar{\nu}_\tau$  processes mediated via  $b \rightarrow c\tau\bar{\nu}_\tau$  quark level transitions. In our previous work [59], we have presented the complete expressions for all the required observables. The  $q^2$  dependence of the helicity

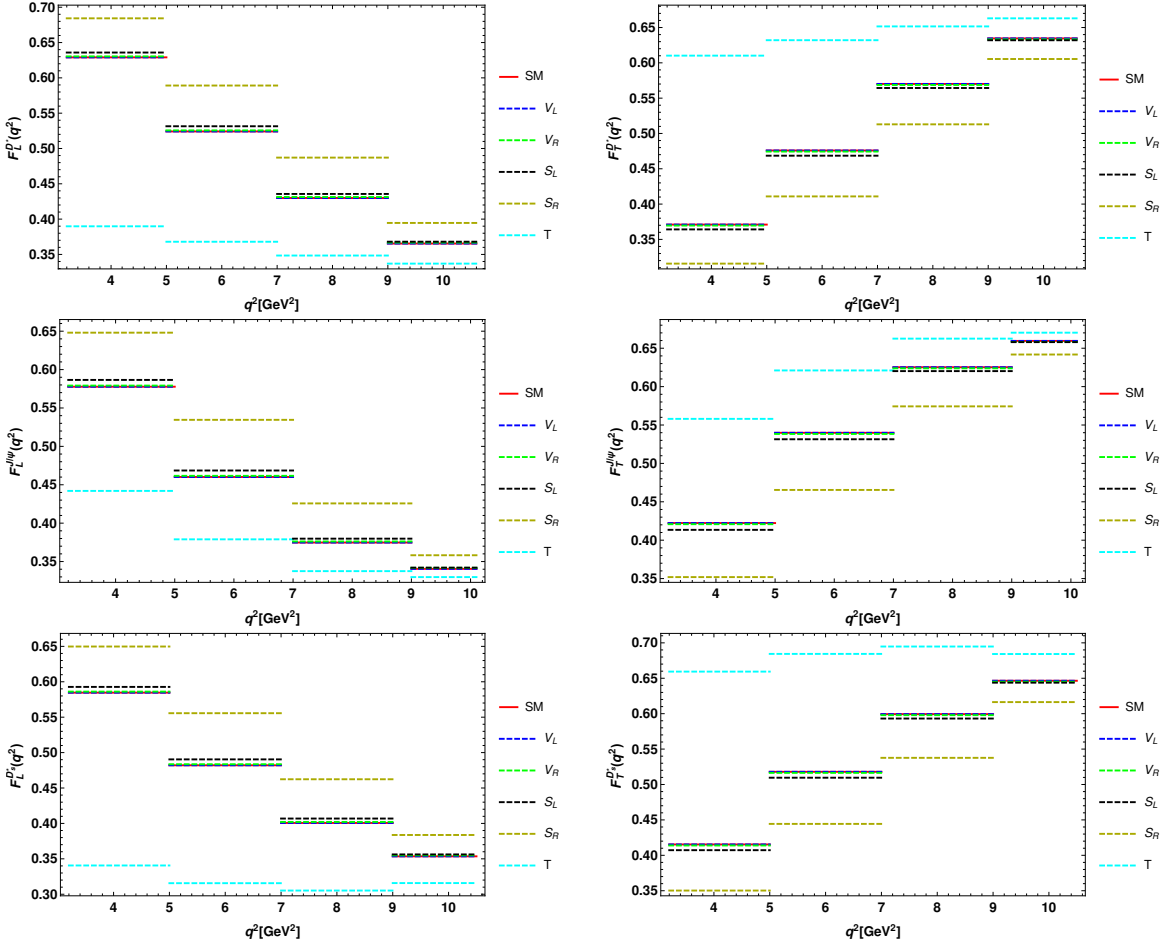


FIG. 12: The bin-wise longitudinal (left panel) and transverse (right panel) polarization asymmetry of daughter vector meson of  $\bar{B} \rightarrow D^* \tau \bar{\nu}_\tau$  (top),  $B_c^+ \rightarrow J/\psi \tau^+ \nu_\tau$  (middle) and  $\bar{B}_s \rightarrow \bar{D}_s^* \tau \bar{\nu}_\tau$  (bottom) processes in four  $q^2$  bin for case B.

form factors of  $\Lambda_b \rightarrow \Lambda_c$ , computed in the lattice QCD approach are taken from [51, 55] and the other remaining input parameters from [72]. Using the best-fit values of individual new real and complex Wilson coefficients from Table I, we show the bin-wise graphical representation of branching ratios (top), forward-backward-asymmetry (second from top),  $R_{\Lambda_c}$  (third from top),  $\tau$ -polarization (fourth from top) and  $\Lambda_c$  polarization (bottom) asymmetries of  $\Lambda_b \rightarrow \Lambda_c \tau \bar{\nu}_\tau$  process in Fig. 18. Here the left (right) panel represents the plots for case A (case B). The presence of  $V_L$  ( $V_R$ ) affects the branching ratio maximally in all the bins (none of the bins) for case A and in the last three bins (last three) for case B, whereas the  $S_L$  contribution is within SM  $1\sigma$  error range. The  $S_R$  has large effects on last two bins for both cases. The new physics contribution to branching ratio, arising due to an additional  $T$  lies within  $1\sigma$  uncertainties range of SM for case A and has larger impact in the first three bins for case B. The inclusion of  $S_R$  coefficient provide profound deviation in  $A_{FB}^{\Lambda_c}$  observable from SM predictions for both cases. The LNU parameters of  $\Lambda_b \rightarrow \Lambda_c$  deviates significantly

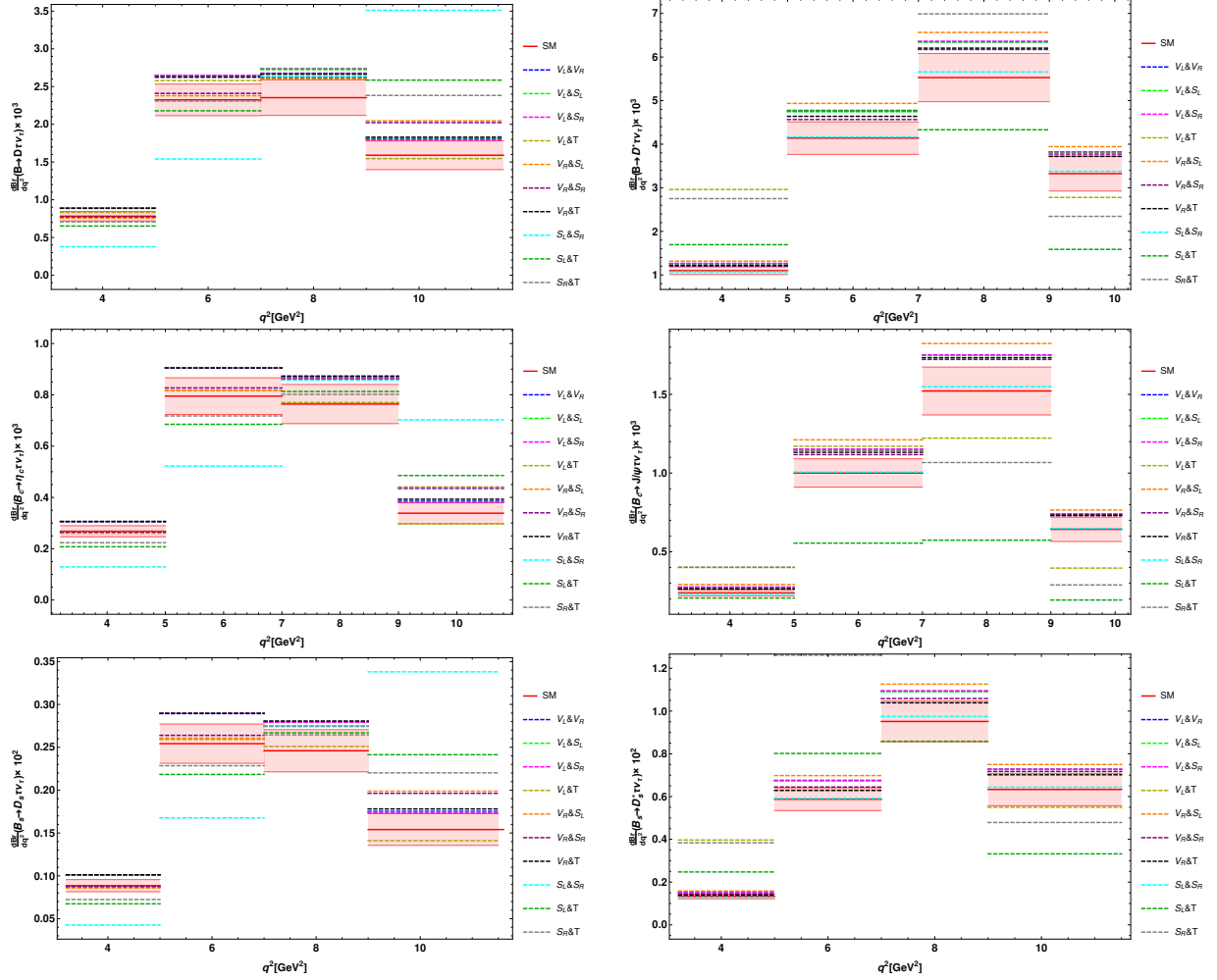


FIG. 13: The bin-wise branching ratios of  $\bar{B} \rightarrow D\tau\bar{\nu}_\tau$  (top-left panel),  $\bar{B} \rightarrow D^*\tau\bar{\nu}_\tau$  (top-right panel),  $B_c^+ \rightarrow \eta_c\tau^+\nu_\tau$  (middle-left panel),  $B_c^+ \rightarrow J/\psi\tau^+\nu_\tau$  (middle-right panel),  $B_s \rightarrow D_s\tau\bar{\nu}_\tau$  (bottom-left panel) and  $\bar{B}_s \rightarrow \bar{D}_s^*\tau\bar{\nu}_\tau$  (bottom-right panel) processes in four  $q^2$  bins for case C.

from SM in last three bins due to an additional coefficients. The real  $V_R$  contribution is less in the 2<sup>nd</sup> bin and the complex  $T$  affects the first bin of  $R_{\Lambda_c}$  profoundly. The new real and complex scalar contributions has shifted the values of  $P_\tau^{\Lambda_c}$  significantly from the SM results and the  $F_L^{\Lambda_c}$  is affected by real  $S_R$  and complex  $V_R/S_R$  coefficients. The bin-wise numerical values for all observables for complex new Wilson coefficients are shown in Table VII. Since,  $F_T = 1 - F_L$ , we don't include the  $F_T^{\Lambda_c}$  values in VII. The bottom panel of Fig. 19 represents the correlation plots of the  $R_{\Lambda_c}$ ,  $P_\tau^{\Lambda_c}$  and  $F_L^{\Lambda_c}$  parameters in the full  $q^2$  range obtained by using the  $1\sigma$  range of new coefficients for case B. The correlation plots of the lepton non-universality parameters of all the discussed  $B \rightarrow P$ ,  $B \rightarrow V$  and  $\Lambda_b \rightarrow \Lambda_c$  processes are graphically presented in Fig. 20. Fig. 21. depicts the bin-wise values for the branching ratio (top-left panel),  $A_{FB}^{\Lambda_c}$  (top-right panel),  $R_{\Lambda_c}$  (middle-left panel),  $P_\tau^{\Lambda_c}$  (middle-right panel) and  $F_L^{\Lambda_c}$  (bottom panel) observables of  $\Lambda_b \rightarrow \Lambda_c$  process graphically for

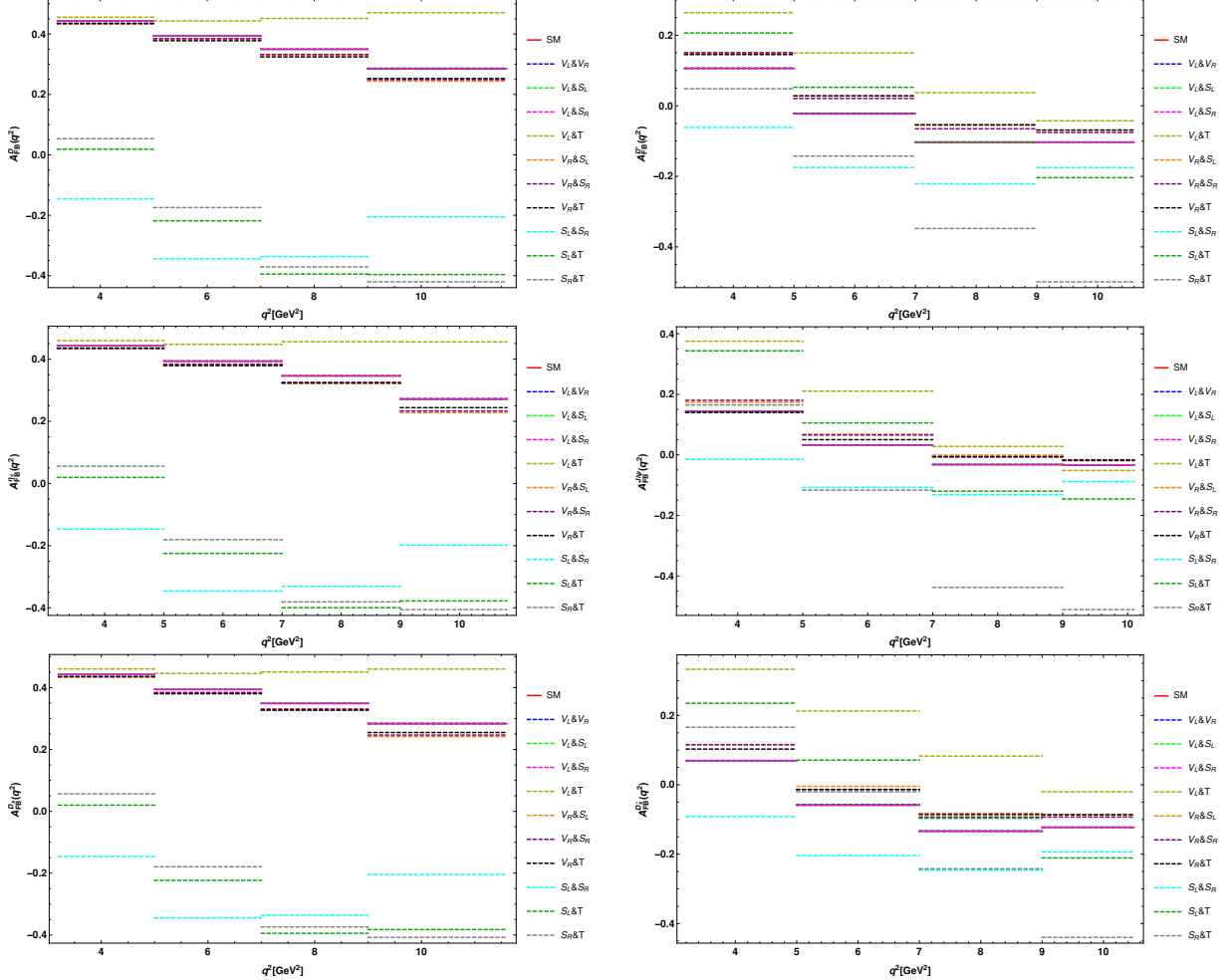


FIG. 14: The bin-wise forward-backward asymmetry of  $\bar{B} \rightarrow D\tau\bar{\nu}_\tau$  (top-left panel),  $\bar{B} \rightarrow D^*\tau\bar{\nu}_\tau$  (top-right panel),  $B_c^+ \rightarrow \eta_c\tau^+\nu_\tau$  (middle-left panel),  $B_c^+ \rightarrow J/\psi\tau^+\nu_\tau$  (middle-right panel),  $B_s \rightarrow D_s\tau\bar{\nu}_\tau$  (bottom-left panel) and  $B_s \rightarrow D_s^*\tau\bar{\nu}_\tau$  (bottom-right panel) processes in four  $q^2$  bins for case C.

case C. We find that,  $V_L \& T$  and  $S_R \& T$  has large impact on all observables, expect minor contribution of  $S_R \& T$  to forward-backward asymmetry. The  $S_L \& S_R$  ( $S_L \& T$ ) affects  $A_{FB}^{\Lambda_c}$ ,  $P_\tau$  and  $F_L^{\Lambda_c}$  ( $A_{FB}^{\Lambda_c}$ ,  $R_{\Lambda_c}$  and  $P_\tau$ ) observables.

## VI. $B \rightarrow D^{**}\tau\bar{\nu}_\tau$ PROCESSES

The implications of additional real and complex coefficients on the lepton non-universality parameters of  $B \rightarrow D^{**}\tau\bar{\nu}_\tau$  processes, where  $D^{**} = \{D_0^*, D_1^*, D_1, D_2^*\}$  are the four lightest excited charmed mesons, will be discussed in this section. The detailed expressions for decay rates in the SM [60] and in the presence of NP can be found in [60, 61]. The lepton

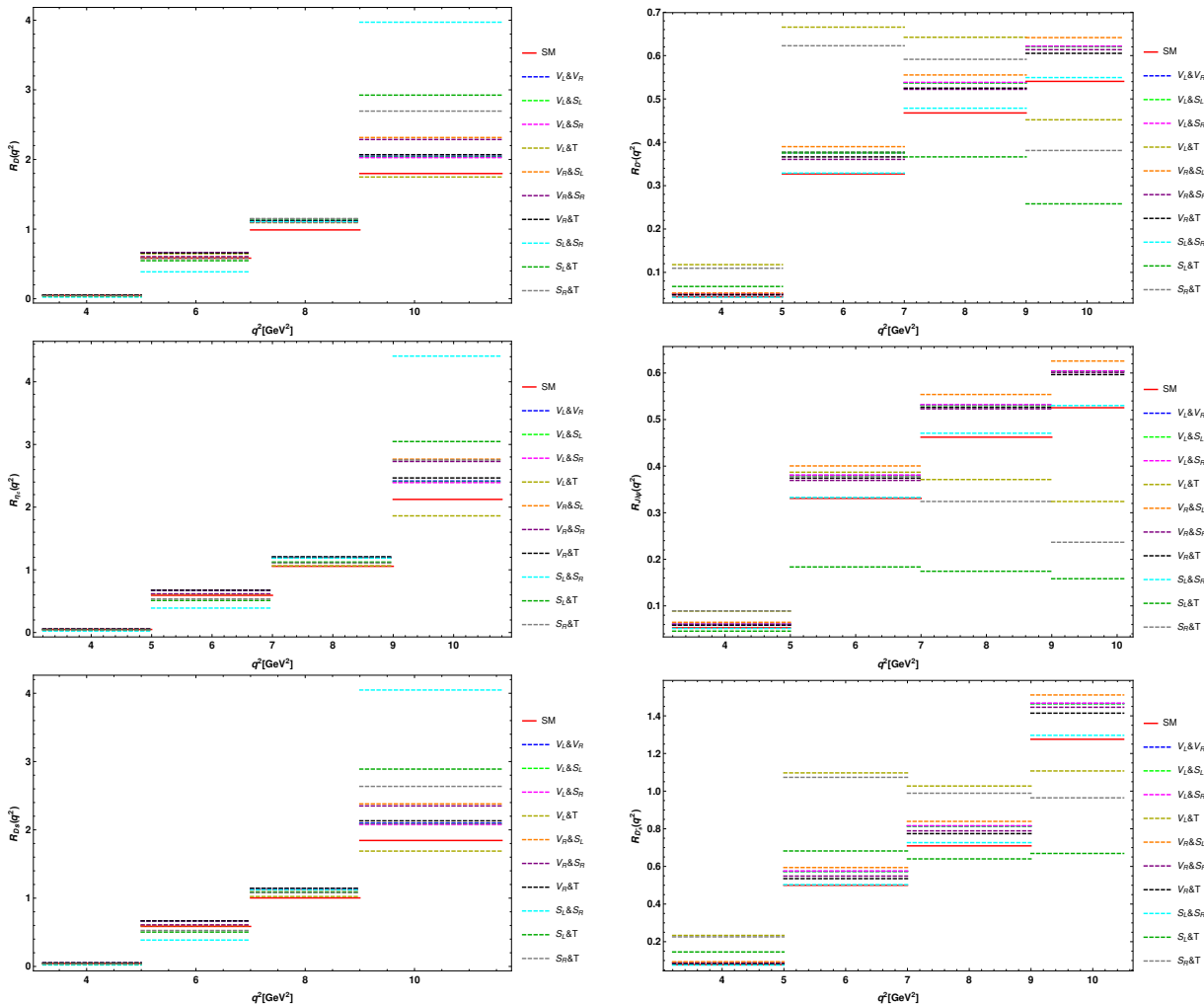


FIG. 15: The bin-wise  $R_D$  (top-left panel),  $R_{D^*}$  (top-right),  $R_{\eta_c}$  (middle-left panel),  $R_{J/\psi}$  (middle-right),  $R_{D_s}$  (bottom-left panel) and  $R_{D_s^*}$  (bottom-right panel) in four  $q^2$  bins for case C.

non-universality ratio  $R_{D^{**}}$  is defined as

$$R_{D^{**}} = \frac{\text{BR}(B \rightarrow D^{**}\tau\nu_\tau)}{\text{BR}(B \rightarrow D^{**}l\nu_l)}, \quad l = e, \mu. \quad (21)$$

We use the input parameters from [72] and the required form factors from [60, 61] for numerical analysis. Using the best-fit values from Table I, the bin-wise graphical representation of  $R_{D_0^*}$  (top-left panel),  $R_{D_1}$  (top-right panel),  $R_{D_1^*}$  (bottom-left panel) and  $R_{D_2^*}$  (bottom-right panel) parameters for case A, case B and case C are shown in Fig. 22, 23 and 24 respectively. For the case of individual real coefficients, the contribution from  $V_L$  provides significant deviation from the SM values of  $R_{D_{0(2)}^*}$ ,  $R_{D_1}$  ratios in the last two bins. The  $V_R$  coefficient has effectively impact on the  $R_{D_{0(2)}^*}$  parameters in the 2<sup>nd</sup> and 3<sup>rd</sup> bins. The  $S_L$  coupling has negligible effects on all LNU parameters except the 2<sup>nd</sup> and 3<sup>rd</sup> bins of  $R_{D_1}$ . One can notice profound deviation in all the parameters in the last two bins due to an additional contribution from  $S_R$  coefficient. Tensor coupling has no effect on  $R_{D_1^*}$  and the first

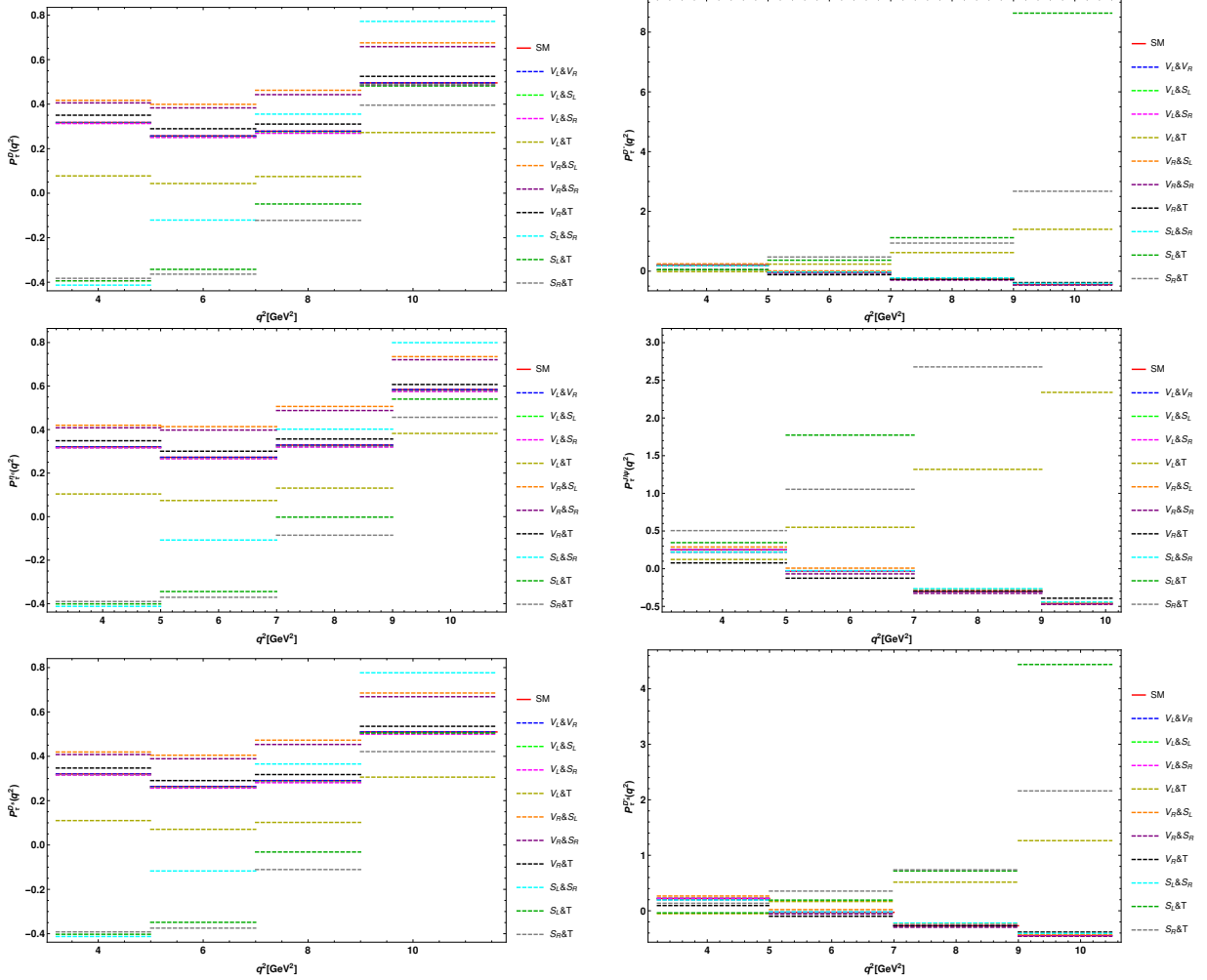


FIG. 16: The bin-wise  $\tau$ -polarization asymmetry of  $\bar{B} \rightarrow D\tau\bar{\nu}_\tau$  (top-left panel),  $\bar{B} \rightarrow D^*\tau\bar{\nu}_\tau$  (top-right panel),  $B_c^+ \rightarrow \eta_c\tau^+\nu_\tau$  (middle-left panel),  $B_c^+ \rightarrow J/\psi\tau^+\nu_\tau$  (middle-right panel),  $B_s \rightarrow D_s\tau\bar{\nu}_\tau$  (bottom-left panel) and  $B_s \rightarrow D_s^*\tau\bar{\nu}_\tau$  (bottom-right panel) processes in four  $q^2$  bins for case C.

$q^2$  bin of remaining three LNU ratios. It should be noted that the  $R_i$ ,  $i = D_0^*, D_1, D_1^*, D_2^*$  parameters have shifted maximally due to the presence of complex  $V_L$  coupling. The deviation due to complex  $V_R$  coefficient is minor in the last two bins of all these LNU parameters. The  $S_R$  ( $T$ ) has large impact on  $R_{D_1}$  ( $R_{D_1^{(*)}}$ ) parameters except in the first bin. Among 10 possible sets of two real coefficients, the  $R_i$  ratios deviate significantly from their respective SM results due to the  $V_L\&T$ ,  $S_L\&T$  and  $S_R\&T$  combinations of coefficients. The last two bins of  $R_{D_1^*}$  significantly deviates from SM values due to an additional contribution from  $S_L\&S_R$  coefficients. The bin-wise numerical values of the ratio for the sum of the four  $D^{**}$  states are given in Table VIII.

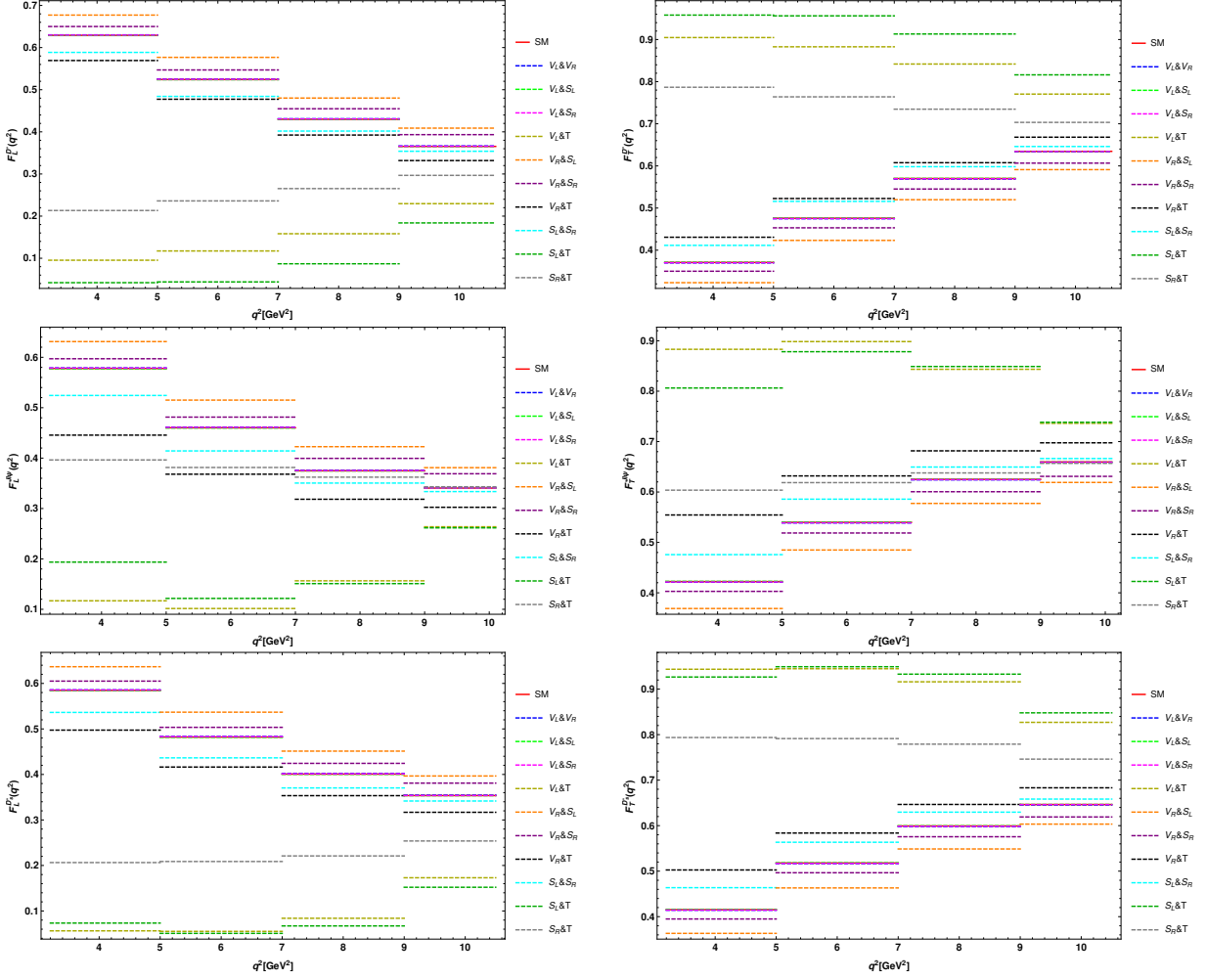


FIG. 17: The bin-wise longitudinal (left panel) and transverse (right panel) polarization asymmetry of daughter vector meson of  $\bar{B} \rightarrow D^* \tau \bar{\nu}_\tau$  (top),  $B_c^+ \rightarrow J/\psi \tau^+ \nu_\tau$  (middle) and  $B_s \rightarrow D_s^* \tau \bar{\nu}_\tau$  (bottom) processes in four  $q^2$  bin for case C.

## VII. CONCLUSION

We have scrutinized the relevant semileptonic decays of  $B$  mesons and  $\Lambda_b$  involving the  $b \rightarrow c \tau \bar{\nu}_\tau$  quark level transition in an effective theory approach. This model independent strategy provides additional vector, scalar and tensor contributions to the standard model result. We have considered three cases of new Wilson coefficients: (a) presence of individual real coupling (b) presence of individual complex coupling and (c) presence of two real couplings and we performed a *chi*-square fitting to extract the best-fit values of these new coefficients, from the experimental data on  $R_{D^{(*)}}$ ,  $R_{J/\psi}$  and  $\text{Br}(B_c^+ \rightarrow \tau^+ \nu_\tau)$  observables. For case C, we have taken all possible combinations of real coefficients (total 10). Using the best-fit values of real/complex Wilson coefficients, we then estimate the branching ratios, forward-backward asymmetry, lepton non-universality, lepton and hadron polarization

TABLE IV: Predicted bin-wise values of branching ratios and forward-backward asymmetries of  $B_{(s)} \rightarrow D_{(s)}^{(*)} \tau \bar{\nu}_\tau$  and  $B_c^+ \rightarrow (\eta_c, J/\psi) \tau^+ \nu_\tau$  processes in the SM and in the presence of new complex Wilson coefficients (case B).

Observables	Values for SM	values for $V_L$	Values for $V_R$	values for $S_L$	Values for $S_R$	Values for $T$
$10^3 \text{ Br}(\bar{B} \rightarrow \bar{D}) _{q^2 \in [m_\tau^2, 5]}$	( $0.782 \pm 0.03$ )	0.896	0.888	0.848	0.61	0.87
$10^3 \text{ Br}(\bar{B} \rightarrow \bar{D}) _{q^2 \in [5, 7]}$	( $2.324 \pm 0.21$ )	2.66	2.64	2.591	2.03	2.62
$10^3 \text{ Br}(\bar{B} \rightarrow \bar{D}) _{q^2 \in [7, 9]}$	( $2.36 \pm 0.24$ )	2.7	2.674	2.74	2.62	2.643
$10^3 \text{ Br}(\bar{B} \rightarrow \bar{D}) _{q^2 \in [9, 11.6]}$	( $1.59 \pm 0.191$ )	1.82	1.81	2.0	2.671	1.73
$\langle A_{FB}^D \rangle _{q^2 \in [m_\tau^2, 5]}$	( $0.443 \pm 0.0354$ )	0.443	0.443	0.4395	0.262	0.448
$\langle A_{FB}^D \rangle _{q^2 \in [5, 7]}$	( $0.394 \pm 0.035$ )	0.394	0.394	0.3896	0.12	0.41
$\langle A_{FB}^D \rangle _{q^2 \in [7, 9]}$	( $0.3494 \pm 0.33$ )	0.3494	0.3494	0.3406	0.0093	0.379
$\langle A_{FB}^D \rangle _{q^2 \in [9, 11.6]}$	( $0.2851 \pm 0.034$ )	0.2851	0.2851	0.2638	-0.0356	0.3326
$10^3 \text{ Br}(\bar{B} \rightarrow \bar{D}^*) _{q^2 \in [m_\tau^2, 5]}$	( $1.1 \pm 0.088$ )	1.258	1.261	1.12	1.29	1.574
$10^3 \text{ Br}(\bar{B} \rightarrow \bar{D}^*) _{q^2 \in [5, 7]}$	( $4.14 \pm 0.373$ )	4.75	4.76	4.2	4.8	5.26
$10^3 \text{ Br}(\bar{B} \rightarrow \bar{D}^*) _{q^2 \in [7, 9]}$	( $5.53 \pm 0.55$ )	6.34	6.352	5.584	6.144	6.123
$10^3 \text{ Br}(\bar{B} \rightarrow \bar{D}^*) _{q^2 \in [9, 11.6]}$	( $3.32 \pm 0.4$ )	3.81	3.82	3.34	3.483	3.242
$\langle A_{FB}^{D^*} \rangle _{q^2 \in [m_\tau^2, 5]}$	( $0.106 \pm 0.009$ )	0.106	0.148	0.115	0.025	0.165
$\langle A_{FB}^{D^*} \rangle _{q^2 \in [5, 7]}$	( $-0.0225 \pm 0.002$ )	-0.0225	0.03	-0.0123	-0.081	0.0261
$\langle A_{FB}^{D^*} \rangle _{q^2 \in [7, 9]}$	( $-0.104 \pm 0.008$ )	-0.104	-0.0493	-0.095	-0.145	-0.0824
$\langle A_{FB}^{D^*} \rangle _{q^2 \in [9, 11.6]}$	( $-0.103 \pm 0.013$ )	-0.103	-0.063	-0.098	-0.132	-0.11
$10^4 \text{ Br}(B_c \rightarrow \eta_c) _{q^2 \in [m_\tau^2, 5]}$	( $2.7 \pm 0.22$ )	3.1	3.05	2.91	2.08	2.94
$10^4 \text{ Br}(B_c \rightarrow \eta_c) _{q^2 \in [5, 7]}$	( $7.95 \pm 0.72$ )	9.11	9.03	8.877	6.93	8.77
$10^4 \text{ Br}(B_c \rightarrow \eta_c) _{q^2 \in [7, 9]}$	( $7.64 \pm 0.611$ )	8.76	8.682	8.96	8.545	8.382
$10^4 \text{ Br}(B_c \rightarrow \eta_c) _{q^2 \in [9, 11.6]}$	( $3.384 \pm 0.41$ )	3.88	3.85	4.3	5.5	3.6
$\langle A_{FB}^{\eta_c} \rangle _{q^2 \in [m_\tau^2, 5]}$	( $0.4429 \pm 0.035$ )	0.4429	0.4429	0.4392	0.262	0.4483
$\langle A_{FB}^{\eta_c} \rangle _{q^2 \in [5, 7]}$	( $0.394 \pm 0.035$ )	0.394	0.394	0.3884	0.12	0.41
$\langle A_{FB}^{\eta_c} \rangle _{q^2 \in [7, 9]}$	( $0.3458 \pm 0.028$ )	0.3458	0.3458	0.3346	-0.01	0.375
$\langle A_{FB}^{\eta_c} \rangle _{q^2 \in [9, 11.6]}$	( $0.27 \pm 0.032$ )	0.27	0.27	0.2483	-0.03	0.315
$10^3 \text{ Br}(B_c \rightarrow J/\psi) _{q^2 \in [m_\tau^2, 5]}$	( $0.24 \pm 0.019$ )	0.274	0.275	0.245	0.287	0.283
$10^3 \text{ Br}(B_c \rightarrow J/\psi) _{q^2 \in [5, 7]}$	( $1.0 \pm 0.09$ )	1.15	1.15	1.02	1.16	1.1
$10^3 \text{ Br}(B_c \rightarrow J/\psi) _{q^2 \in [7, 9]}$	( $1.52 \pm 0.132$ )	1.74	1.75	1.534	1.66	1.463
$10^3 \text{ Br}(B_c \rightarrow J/\psi) _{q^2 \in [9, 11.6]}$	( $0.643 \pm 0.077$ )	0.737	0.74	0.644	0.661	0.589
$\langle A_{FB}^{J/\psi} \rangle _{q^2 \in [m_\tau^2, 5]}$	( $0.1434 \pm 0.012$ )	0.1434	0.172	0.15	0.058	0.219
$\langle A_{FB}^{J/\psi} \rangle _{q^2 \in [5, 7]}$	( $0.032 \pm 0.003$ )	0.032	0.066	0.04	-0.029	0.07
$\langle A_{FB}^{J/\psi} \rangle _{q^2 \in [7, 9]}$	( $-0.032 \pm 0.0026$ )	-0.032	$-4.9 \times 10^{-4}$	-0.0254	-0.073	-0.0334
$\langle A_{FB}^{J/\psi} \rangle _{q^2 \in [9, 11.6]}$	( $-0.0345 \pm 0.0042$ )	-0.0345	-0.015	-0.031	-0.059	-0.046
$10^3 \text{ Br}(B_s \rightarrow D_s) _{q^2 \in [m_\tau^2, 5]}$	( $0.86 \pm 0.69$ )	1.02	1.0	0.96	0.687	0.966
$10^3 \text{ Br}(B_s \rightarrow D_s) _{q^2 \in [5, 7]}$	( $2.542 \pm 0.23$ )	2.92	2.89	2.836	2.22	2.8
$10^3 \text{ Br}(B_s \rightarrow D_s) _{q^2 \in [7, 9]}$	( $2.46 \pm 0.23$ )	2.82	2.8	2.87	2.74	2.71
$10^3 \text{ Br}(B_s \rightarrow D_s) _{q^2 \in [9, 11.6]}$	( $1.54 \pm 0.185$ )	1.77	1.75	1.95	2.58	1.65
$\langle A_{FB}^{D_s} \rangle _{q^2 \in [m_\tau^2, 5]}$	( $0.443 \pm 0.0354$ )	0.443	0.443	0.44	0.263	0.449
$\langle A_{FB}^{D_s} \rangle _{q^2 \in [5, 7]}$	( $0.4 \pm 0.036$ )	0.4	0.4	0.3893	0.12	0.41
$\langle A_{FB}^{D_s} \rangle _{q^2 \in [7, 9]}$	( $0.349 \pm 0.032$ )	0.349	0.349	0.34	0.0096	0.377
$\langle A_{FB}^{D_s} \rangle _{q^2 \in [9, 11.6]}$	( $0.2833 \pm 0.034$ )	0.2833	0.2833	0.262	-0.035	0.327
$10^3 \text{ Br}(B_s \rightarrow D_s^*) _{q^2 \in [m_\tau^2, 5]}$	( $1.325 \pm 0.1$ )	1.52	1.53	1.35	1.572	2.02
$10^3 \text{ Br}(B_s \rightarrow D_s^*) _{q^2 \in [5, 7]}$	( $5.88 \pm 0.53$ )	6.74	6.75	5.97	6.85	7.77
$10^3 \text{ Br}(B_s \rightarrow D_s^*) _{q^2 \in [7, 9]}$	( $9.515 \pm 0.86$ )	10.1	10.1	9.614	10.6	10.8
$10^3 \text{ Br}(B_s \rightarrow D_s^*) _{q^2 \in [9, 11.6]}$	( $6.33 \pm 0.76$ )	7.2	7.28	6.36	6.64	6.25
$\langle A_{FB}^{D_s^*} \rangle _{q^2 \in [m_\tau^2, 5]}$	( $0.07 \pm 0.006$ )	0.07	0.12	0.078	-0.004	0.184
$\langle A_{FB}^{D_s^*} \rangle _{q^2 \in [5, 7]}$	( $-0.0584 \pm 0.0053$ )	-0.0584	$7.88 \times 10^{-4}$	-0.048	-0.11	0.0342
$\langle A_{FB}^{D_s^*} \rangle _{q^2 \in [7, 9]}$	( $-0.134 \pm 0.12$ )	-0.134	-0.073	-0.125	-0.17	-0.0872
$\langle A_{FB}^{D_s^*} \rangle _{q^2 \in [9, 11.6]}$	( $-0.123 \pm 0.015$ )	-0.123	-0.077	-0.1174	-0.15	-0.119

TABLE V: Predicted bin-wise values of LNU ratios and  $\tau$ -polarization asymmetries of  $B_{(s)} \rightarrow D_{(s)}^{(*)}\tau\bar{\nu}_\tau$  and  $B_c^+ \rightarrow (\eta_c, J/\psi)\tau^+\nu_\tau$  processes in the SM and in the presence of new complex Wilson coefficients (case B).

Observables	Values for SM	values for $V_L$	Values for $V_R$	values for $V_L$	Values for $V_R$	Values for $T$
$\langle R_D \rangle _{q^2 \in [m_\tau^2, 5]}$	0.048	0.055	0.054	0.052	0.037	0.053
$\langle R_D \rangle _{q^2 \in [5, 7]}$	0.583	0.668	0.662	0.65	0.51	0.655
$\langle R_D \rangle _{q^2 \in [7, 9]}$	0.989	1.133	1.123	1.151	1.101	1.11
$\langle R_D \rangle _{q^2 \in [9, 11.6]}$	1.8	2.061	2.043	2.27	3.02	1.954
$\langle P_\tau^D \rangle _{q^2 \in [m_\tau^2, 5]}$	0.318	0.318	0.318	0.37	0.12	0.26
$\langle P_\tau^D \rangle _{q^2 \in [5, 7]}$	0.2572	0.2572	0.2572	0.334	0.15	0.199
$\langle P_\tau^D \rangle _{q^2 \in [7, 9]}$	0.2783	0.2783	0.2783	0.38	0.352	0.223
$\langle P_\tau^D \rangle _{q^2 \in [9, 11.6]}$	0.4955	0.4955	0.4955	0.6	0.7	0.44
$\langle R_{D^*} \rangle _{q^2 \in [m_\tau^2, 5]}$	0.044	0.05	0.0502	0.045	0.052	0.063
$\langle R_{D^*} \rangle _{q^2 \in [5, 7]}$	0.33	0.375	0.376	0.332	0.379	0.416
$\langle R_{D^*} \rangle _{q^2 \in [7, 9]}$	0.468	0.536	0.538	0.472	0.52	0.518
$\langle R_{D^*} \rangle _{q^2 \in [9, 11.6]}$	0.54	0.62	0.622	0.543	0.567	0.527
$\langle P_\tau^{D^*} \rangle _{q^2 \in [m_\tau^2, 5]}$	0.205	0.205	0.206	0.225	0.361	0.116
$\langle P_\tau^{D^*} \rangle _{q^2 \in [5, 7]}$	-0.036	-0.036	-0.036	-0.0119	0.165	0.11
$\langle P_\tau^{D^*} \rangle _{q^2 \in [7, 9]}$	-0.2716	-0.2716	-0.271	-0.2508	-0.0754	0.682
$\langle P_\tau^{D^*} \rangle _{q^2 \in [9, 11.6]}$	-0.4484	-0.4484	-0.4483	-0.4382	-0.338	-0.013
$\langle R_{\eta_c} \rangle _{q^2 \in [m_\tau^2, 5]}$	0.049	0.056	0.0556	0.053	0.038	0.0381
$\langle R_{\eta_c} \rangle _{q^2 \in [5, 7]}$	0.593	0.68	0.674	0.663	0.517	0.654
$\langle R_{\eta_c} \rangle _{q^2 \in [7, 9]}$	1.06	1.211	1.2	1.24	1.181	1.16
$\langle R_{\eta_c} \rangle _{q^2 \in [9, 11.6]}$	2.13	2.44	2.41	2.7	3.436	2.254
$\langle P_\tau^{\eta_c} \rangle _{q^2 \in [m_\tau^2, 5]}$	0.3205	0.3205	0.3205	0.3733	0.123	0.266
$\langle P_\tau^{\eta_c} \rangle _{q^2 \in [5, 7]}$	0.2725	0.2725	0.2725	0.349	0.166	0.2214
$\langle P_\tau^{\eta_c} \rangle _{q^2 \in [7, 9]}$	0.3287	0.3287	0.3287	0.428	0.4	0.278
$\langle P_\tau^{\eta_c} \rangle _{q^2 \in [9, 11.6]}$	0.584	0.584	0.584	0.673	0.743	0.538
$\langle R_{J/\psi} \rangle _{q^2 \in [m_\tau^2, 5]}$	0.053	0.061	0.061	0.054	0.064	0.063
$\langle R_{J/\psi} \rangle _{q^2 \in [5, 7]}$	0.331	0.38	0.38	0.336	0.384	0.349
$\langle R_{J/\psi} \rangle _{q^2 \in [7, 9]}$	0.4622	0.53	0.531	0.466	0.503	0.445
$\langle R_{J/\psi} \rangle _{q^2 \in [9, 11.6]}$	0.526	0.602	0.604	0.527	0.54	0.482
$\langle P_\tau^{J/\psi} \rangle _{q^2 \in [m_\tau^2, 5]}$	0.25	0.25	0.25	0.272	0.412	0.24
$\langle P_\tau^{J/\psi} \rangle _{q^2 \in [5, 7]}$	-0.0343	-0.0343	-0.0339	-0.01	0.168	0.182
$\langle P_\tau^{J/\psi} \rangle _{q^2 \in [7, 9]}$	-0.3034	-0.3034	-0.3032	-0.286	-0.137	0.076
$\langle P_\tau^{J/\psi} \rangle _{q^2 \in [9, 11.6]}$	-0.4644	-0.4644	-0.4644	-0.4584	-0.4	-0.02
$\langle R_{D_s} \rangle _{q^2 \in [m_\tau^2, 5]}$	0.046	0.053	0.052	0.05	0.0354	0.05
$\langle R_{D_s} \rangle _{q^2 \in [5, 7]}$	0.586	0.672	0.666	0.653	0.511	0.645
$\langle R_{D_s} \rangle _{q^2 \in [7, 9]}$	1.0	1.15	1.14	1.17	1.12	1.1
$\langle R_{D_s} \rangle _{q^2 \in [9, 11.6]}$	1.844	2.114	2.1	2.332	3.1	1.977
$\langle P_\tau^{D_s} \rangle _{q^2 \in [m_\tau^2, 5]}$	0.32	0.32	0.32	0.373	0.123	0.268
$\langle P_\tau^{D_s} \rangle _{q^2 \in [5, 7]}$	0.2634	0.2634	0.2634	0.3397	0.156	0.214
$\langle P_\tau^{D_s} \rangle _{q^2 \in [7, 9]}$	0.29	0.29	0.29	0.39	0.363	0.242
$\langle P_\tau^{D_s} \rangle _{q^2 \in [9, 11.6]}$	0.51	0.51	0.51	0.612	0.71	0.462
$\langle R_{D_s^*} \rangle _{q^2 \in [m_\tau^2, 5]}$	0.078	0.0894	0.0896	0.08	0.093	0.119
$\langle R_{D_s^*} \rangle _{q^2 \in [5, 7]}$	0.5	0.573	0.574	0.51	0.583	0.661
$\langle R_{D_s^*} \rangle _{q^2 \in [7, 9]}$	0.71	0.813	0.815	0.717	0.79	0.81
$\langle R_{D_s^*} \rangle _{q^2 \in [9, 11.6]}$	0.812	0.931	0.933	0.82	0.852	0.8
$\langle P_\tau^{D_s^*} \rangle _{q^2 \in [m_\tau^2, 5]}$	0.223	0.223	0.225	0.2435	0.382	0.092
$\langle P_\tau^{D_s^*} \rangle _{q^2 \in [5, 7]}$	-0.028	-0.028	-0.0273	-0.0028	0.178	0.082
$\langle P_\tau^{D_s^*} \rangle _{q^2 \in [7, 9]}$	-0.27	-0.27	-0.27	-0.248	-0.07	0.038
$\langle P_\tau^{D_s^*} \rangle _{q^2 \in [9, 11.6]}$	-0.447	-0.47	-0.446	-0.436	-0.334	-0.03

TABLE VI: Predicted bin-wise values of longitudinal polarization asymmetries of daughter meson of  $B_{(s)} \rightarrow D_{(s)}^* \tau \bar{\nu}_\tau$  and  $B_c^+ \rightarrow J/\psi \tau^+ \nu_\tau$  processes in the SM and in the presence of new complex Wilson coefficients (case B).

Observables	Values for SM	values for $V_L$	Values for $V_R$	values for $V_L$	Values for $V_R$	Values for $T$
$\langle F_L^{D^*} \rangle _{q^2 \in [m_\tau^2, 5]}$	$(0.629 \pm 0.023)$	0.629	0.63	0.6359	0.6843	0.39
$\langle F_L^{D^*} \rangle _{q^2 \in [5, 7]}$	$(0.5242 \pm 0.047)$	0.5242	0.526	0.5315	0.589	0.368
$\langle F_L^{D^*} \rangle _{q^2 \in [7, 9]}$	$(0.43 \pm 0.04)$	0.43	0.432	0.436	0.4871	0.35
$\langle F_L^{D^*} \rangle _{q^2 \in [9, 11.6]}$	$(0.3654 \pm 0.044)$	0.3654	0.37	0.368	0.395	0.337
$\langle F_L^{J/\psi} \rangle _{q^2 \in [m_\tau^2, 5]}$	$(0.5777 \pm 0.046)$	0.5777	0.5792	0.5865	0.648	0.442
$\langle F_L^{J/\psi} \rangle _{q^2 \in [5, 7]}$	$(0.46 \pm 0.041)$	0.46	0.462	0.469	0.54	0.379
$\langle F_L^{J/\psi} \rangle _{q^2 \in [7, 9]}$	$(0.3748 \pm 0.032)$	0.3748	0.386	0.38	0.426	0.338
$\langle F_L^{J/\psi} \rangle _{q^2 \in [9, 11.6]}$	$(0.3405 \pm 0.041)$	0.3405	0.342	0.342	0.358	0.33
$\langle F_L^{D_s^*} \rangle _{q^2 \in [m_\tau^2, 5]}$	$(0.585 \pm 0.047)$	0.585	0.586	0.593	0.65	0.341
$\langle F_L^{D_s^*} \rangle _{q^2 \in [5, 7]}$	$(0.482 \pm 0.044)$	0.482	0.484	0.49	0.556	0.32
$\langle F_L^{D_s^*} \rangle _{q^2 \in [7, 9]}$	$(0.4 \pm 0.035)$	0.4	0.402	0.41	0.463	0.31
$\langle F_L^{D_s^*} \rangle _{q^2 \in [9, 11.6]}$	$(0.354 \pm 0.043)$	0.354	0.355	0.3562	0.384	0.32

asymmetries of  $\bar{B} \rightarrow D^{(*)} \tau \bar{\nu}_\tau$ ,  $B_c^+ \rightarrow (\eta_c, J/\psi) \tau^+ \nu_\tau$ ,  $B_s \rightarrow D_s^{(*)} \tau \bar{\nu}_\tau$  and  $\Lambda_b \rightarrow \Lambda_c \tau \bar{\nu}_\tau$  decay processes in four  $q^2$  (in  $\text{GeV}^2$ ) bins:  $m_\tau^2 \rightarrow 5$ ,  $5 \rightarrow 7$ ,  $7 \rightarrow 9$  and  $9 \rightarrow (M_B - M_{P(V)})^2$ . We have also shown the implication of new coefficients on  $\bar{B} \rightarrow D^{**} \tau \bar{\nu}_\tau$  channel, where  $D^{**} = \{D_0^*, D_1^*, D_1, D_2^*\}$  are the four lightest excited charm mesons. As per our main goal, we have checked which type of new couplings are more sensitive to which angular observables of  $b \rightarrow c \tau \bar{\nu}_\tau$  processes and specifically to which  $q^2$  bins. The forward-backward asymmetry of  $B \rightarrow P$  channels are independent of  $V_L$  coefficients and the dependence of vector couplings drops out in  $\tau$ -polarization asymmetry parameters. We noticed that the impacts of only real  $S_R$  coefficient on almost all the angular observables of  $B \rightarrow P(V)$  processes are comparatively larger in all four  $q^2$  bins (minor in the first bin). For the presence of either complex  $S_R$  or  $T$  coefficient, we observed significant deviation in the angular observables from their respective SM results. The effects of complex  $S_L$  coupling on some of the angular observables are found to be larger. The presence of real/complex vector type coefficients also provide profound deviation in some angular observables in different  $q^2$  bins (complex  $V_R$  provides better impacts on observable compared to complex  $V_L$ ). Though real/complex  $S_R$  coefficient is playing a significant role in all observables, the best-fit values of real/complex  $S_R$  doesn't lead to the best  $\chi^2_{\min}/\text{d.o.f.}$  value. Out of all possible combinations of two real coefficients, the branching ratios and angular observables of  $b \rightarrow c \tau \bar{\nu}_\tau$  decay modes provide comparatively significant deviation from their corresponding SM predictions in the presence of  $S_L \& S_R$ ,  $S_L \& T$  and  $S_R \& T$  sets of coefficients. Other possible sets also have dominant im-

TABLE VII: Predicted bin-wise values of branching ratio and angular observables of  $\Lambda_b \rightarrow \Lambda_c \tau \bar{\nu}_\tau$  process in the SM and in the presence of new complex Wilson coefficients (case B).

Observables	Values for SM	values for $V_L$	Values for $V_R$	values for $V_L$	Values for $V_R$	Values for $T$
$10^3 \text{ Br}(\Lambda_b \rightarrow \Lambda_c) _{q^2 \in [m_\tau^2, 5]}$	$(1.08 \pm 0.09)$	1.233	1.23	1.123	1.08	1.54
$10^3 \text{ Br}(\Lambda_b \rightarrow \Lambda_c) _{q^2 \in [5, 7]}$	$(4.4 \pm 0.396)$	5.05	5.04	4.62	4.6	5.67
$10^3 \text{ Br}(\Lambda_b \rightarrow \Lambda_c) _{q^2 \in [7, 9]}$	$(6.53 \pm 0.653)$	7.481	7.476	6.863	7.2	7.46
$10^3 \text{ Br}(\Lambda_b \rightarrow \Lambda_c) _{q^2 \in [9, 11.6]}$	$(5.6 \pm 0.672)$	6.42	6.424	5.9	6.51	5.635
$\langle A_{FB}^{\Lambda_c} \rangle _{q^2 \in [m_\tau^2, 5]}$	$(0.263 \pm 0.02)$	0.263	0.286	0.271	0.21	0.277
$\langle A_{FB}^{\Lambda_c} \rangle _{q^2 \in [5, 7]}$	$(0.104 \pm 0.009)$	0.103	0.14	0.1184	0.039	0.14
$\langle A_{FB}^{\Lambda_c} \rangle _{q^2 \in [7, 9]}$	$(-0.0114 \pm 0.001)$	-0.0114	0.0324	0.0067	-0.06	0.0263
$\langle A_{FB}^{\Lambda_c} \rangle _{q^2 \in [9, 11.6]}$	$(-0.056 \pm 0.0067)$	-0.056	-0.0213	-0.0422	-0.08	-0.032
$\langle R_{\Lambda_c} \rangle _{q^2 \in [m_\tau^2, 5]}$	0.0536	0.0615	0.0613	0.056	0.054	0.0767
$\langle R_{\Lambda_c} \rangle _{q^2 \in [5, 7]}$	0.377	0.433	0.432	0.396	0.395	0.486
$\langle R_{\Lambda_c} \rangle _{q^2 \in [7, 9]}$	0.539	0.617	0.617	0.566	0.595	0.616
$\langle R_{\Lambda_c} \rangle _{q^2 \in [9, 11.6]}$	0.63	0.722	0.723	0.664	0.733	0.34
$\langle P_\tau^{\Lambda_c} \rangle _{q^2 \in [m_\tau^2, 5]}$	0.0725	0.0725	0.0715	0.11	0.0533	0.063
$\langle P_\tau^{\Lambda_c} \rangle _{q^2 \in [5, 7]}$	-0.174	-0.174	-0.176	-0.1195	-0.127	-0.161
$\langle P_\tau^{\Lambda_c} \rangle _{q^2 \in [7, 9]}$	-0.351	-0.351	-0.353	-0.2846	-0.226	-0.333
$\langle P_\tau \rangle _{q^2 \in [9, 11.6]}$	-0.474	-0.474	-0.4765	-0.4	-0.263	-0.465
$\langle F_L^{\Lambda_c} \rangle _{q^2 \in [m_\tau^2, 5]}$	-0.946	-0.946	-0.71	-0.943	-0.722	-0.923
$\langle F_L^{\Lambda_c} \rangle _{q^2 \in [5, 7]}$	-0.892	-0.892	-0.67	-0.8865	-0.632	-0.892
$\langle F_L^{\Lambda_c} \rangle _{q^2 \in [7, 9]}$	-0.7846	-0.7846	-0.587	-0.778	-0.487	-0.803
$\langle F_L^{\Lambda_c} \rangle _{q^2 \in [9, 11.6]}$	-0.5	-0.5	-0.375	-0.496	-0.279	-0.525

TABLE VIII: Predicted bin-wise values of  $R_{D^{**}}$  parameter in the SM and in the presence of new complex Wilson coefficients.

Model	$R_{D^{**}}(q^2 \in [m_\tau^2, 5])$	$R_{D^{**}}(q^2 \in [5, 7])$	$R_{D^{**}}(q^2 \in [7, (m_B - m_i)^2])$
SM	0.026	0.368	0.526
Only $V_L$	0.177	2.523	3.61
Only $V_R$	0.028	0.353	0.426
Only $S_L$	0.026	0.368	0.528
Only $S_R$	0.033	0.521	0.825
Only $T$	0.038	0.559	0.84

pact on branching ratios and some angular observables of  $b \rightarrow c\tau\bar{\nu}_\tau$  and can accommodate the experimental limit. We have also shown the correlation between the LNU ratios, tau and hadron polarization asymmetry of  $B \rightarrow P(V)$  and  $\Lambda_b \rightarrow \Lambda_c$  processes. To conclude, we have performed a model independent analysis of  $b \rightarrow c\tau\bar{\nu}_\tau$  decay processes and inspected

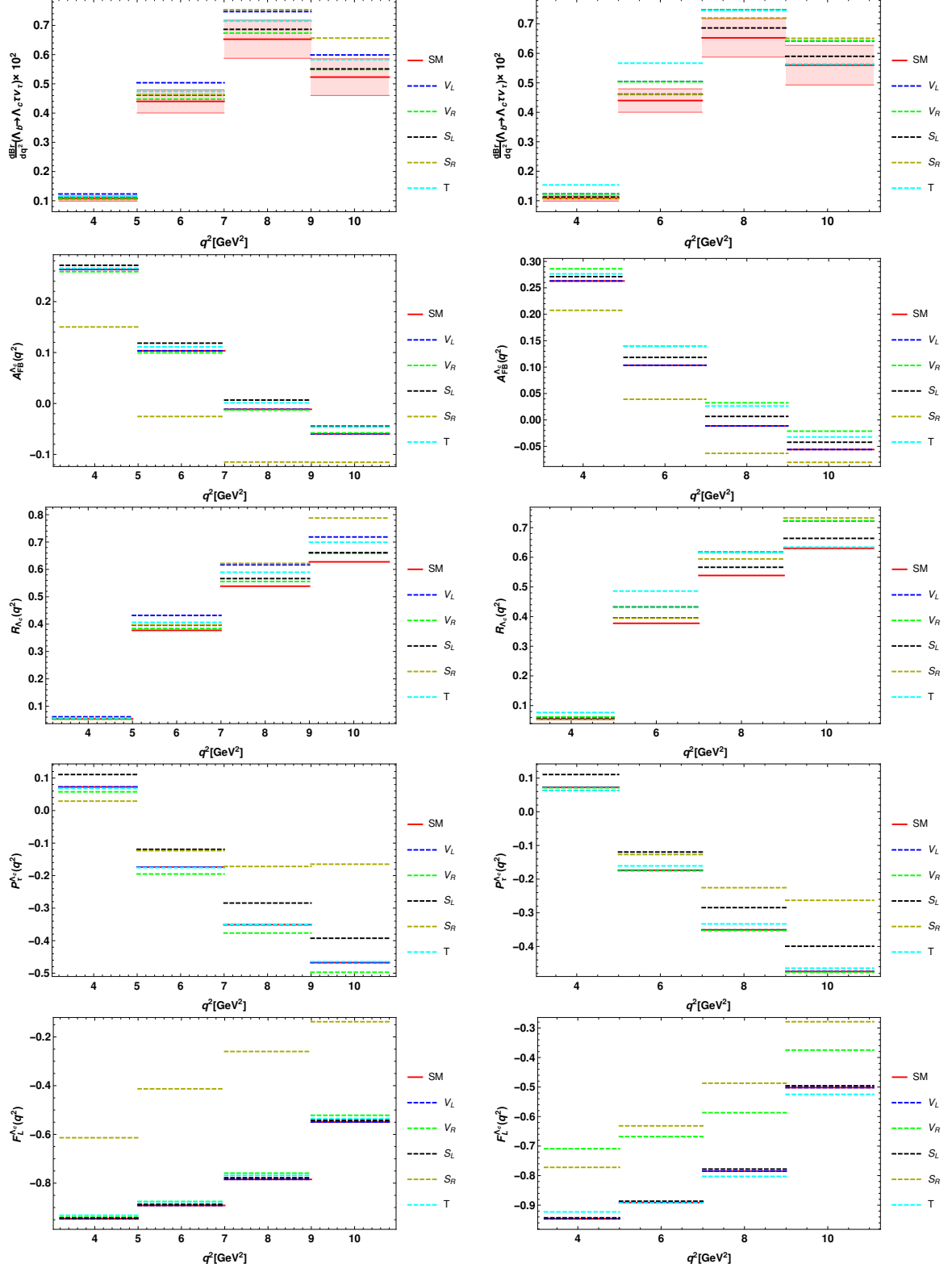


FIG. 18: The bin-wise branching ratio (top), forward-backward asymmetry (second from top),  $R_{\Lambda_c}$  (third from top), tau (fourth from top) and  $\Lambda_c$  (bottom) longitudinal polarization asymmetry of  $\Lambda_b \rightarrow \Lambda_c \tau \bar{\nu}_\tau$  in four  $q^2$  bins for case A (left panel) and case B (right panel).

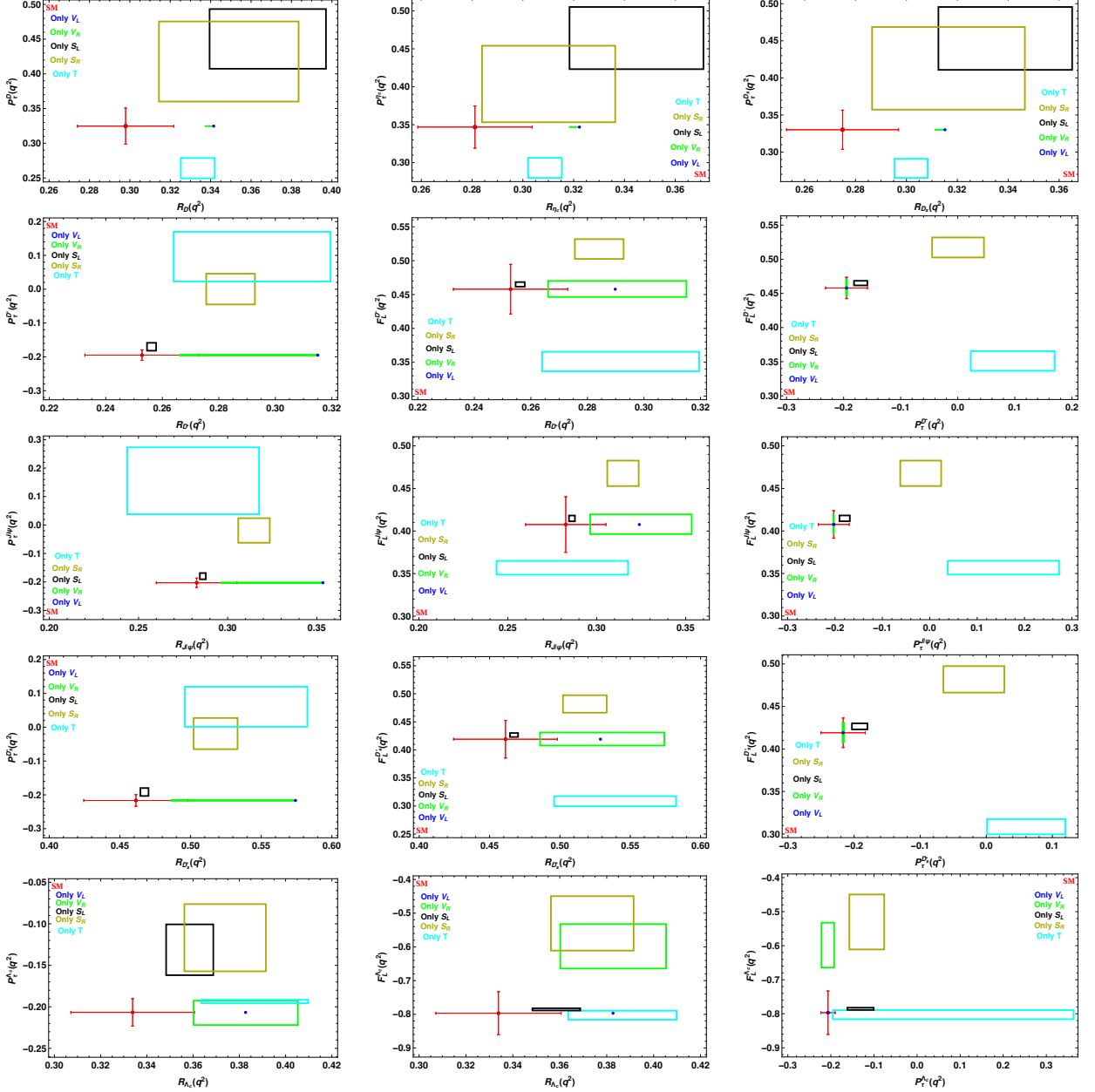


FIG. 19: Correlation between various angular observables of  $b \rightarrow c\tau\bar{\nu}_\tau$  decays for case B.

the branching ratio and angular observables of these channels for both real and complex couplings in four  $q^2$  bins. We have shown the bin-wise sensitivity of new coefficients on angular observables which will provide a clear idea on the structure of new physics.

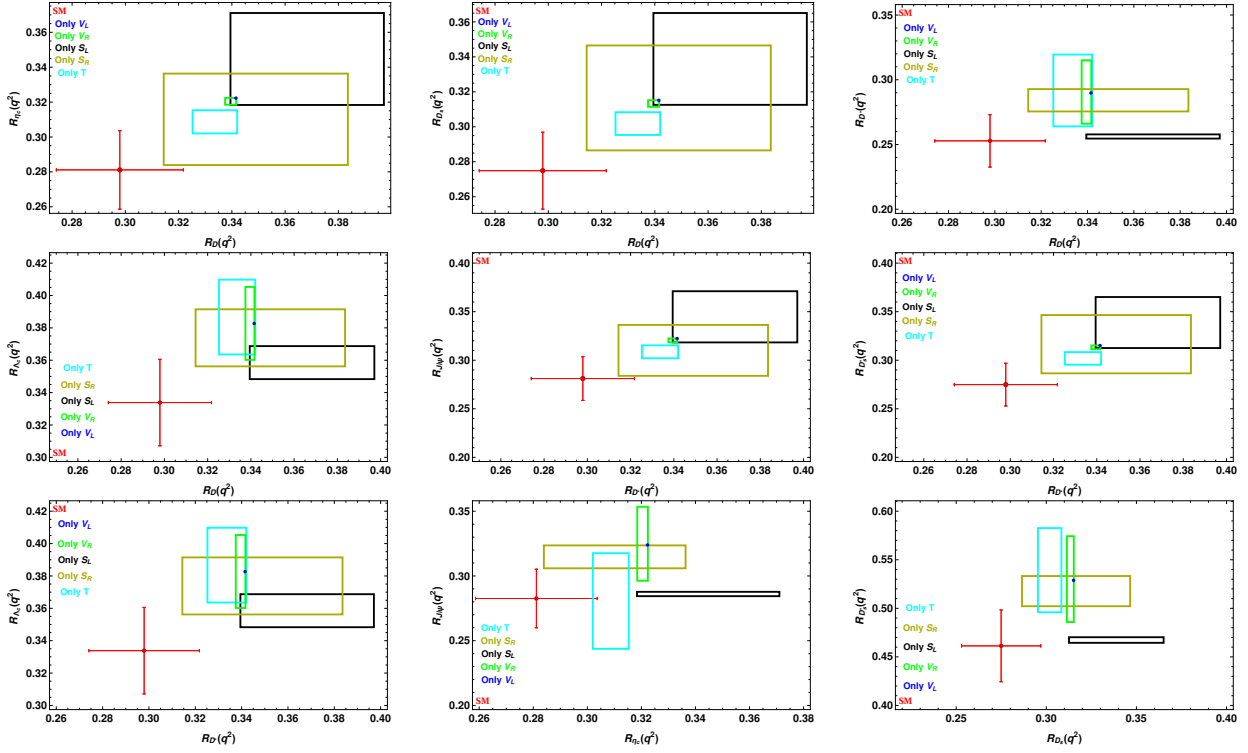


FIG. 20: Correlation between varrious lepton non-universality parameters for case B.

## Acknowledgments

RM would like to thank Science and Engineering Research Board (SERB), Government of India for financial support through grant No. EMR/2017/001448.

- [1] R. Aaij et al. (LHCb), Phys. Rev. Lett. **113**, 151601 (2014), 1406.6482.
- [2] R. Aaij et al. (LHCb) (2019), 1903.09252.
- [3] R. Aaij et al. (LHCb), JHEP **08**, 055 (2017), 1705.05802.
- [4] A. Abdesselam et al. (Belle) (2019), 1904.02440.
- [5] M. Huschle et al. (Belle), Phys. Rev. **D92**, 072014 (2015), 1507.03233.
- [6] A. Abdesselam et al. (Belle), in *Proceedings, 51st Rencontres de Moriond on Electroweak Interactions and Unified Theories: La Thuile, Italy, March 12-19, 2016* (2016), 1603.06711, URL <http://inspirehep.net/record/1431982/files/arXiv:1603.06711.pdf>.
- [7] A. Abdesselam et al. (2016), 1608.06391.
- [8] S. Hirose et al. (Belle), Phys. Rev. **D97**, 012004 (2018), 1709.00129.
- [9] S. Hirose et al. (Belle), Phys. Rev. Lett. **118**, 211801 (2017), 1612.00529.
- [10] R. Aaij et al. (LHCb), Phys. Rev. Lett. **120**, 121801 (2018), 1711.05623.

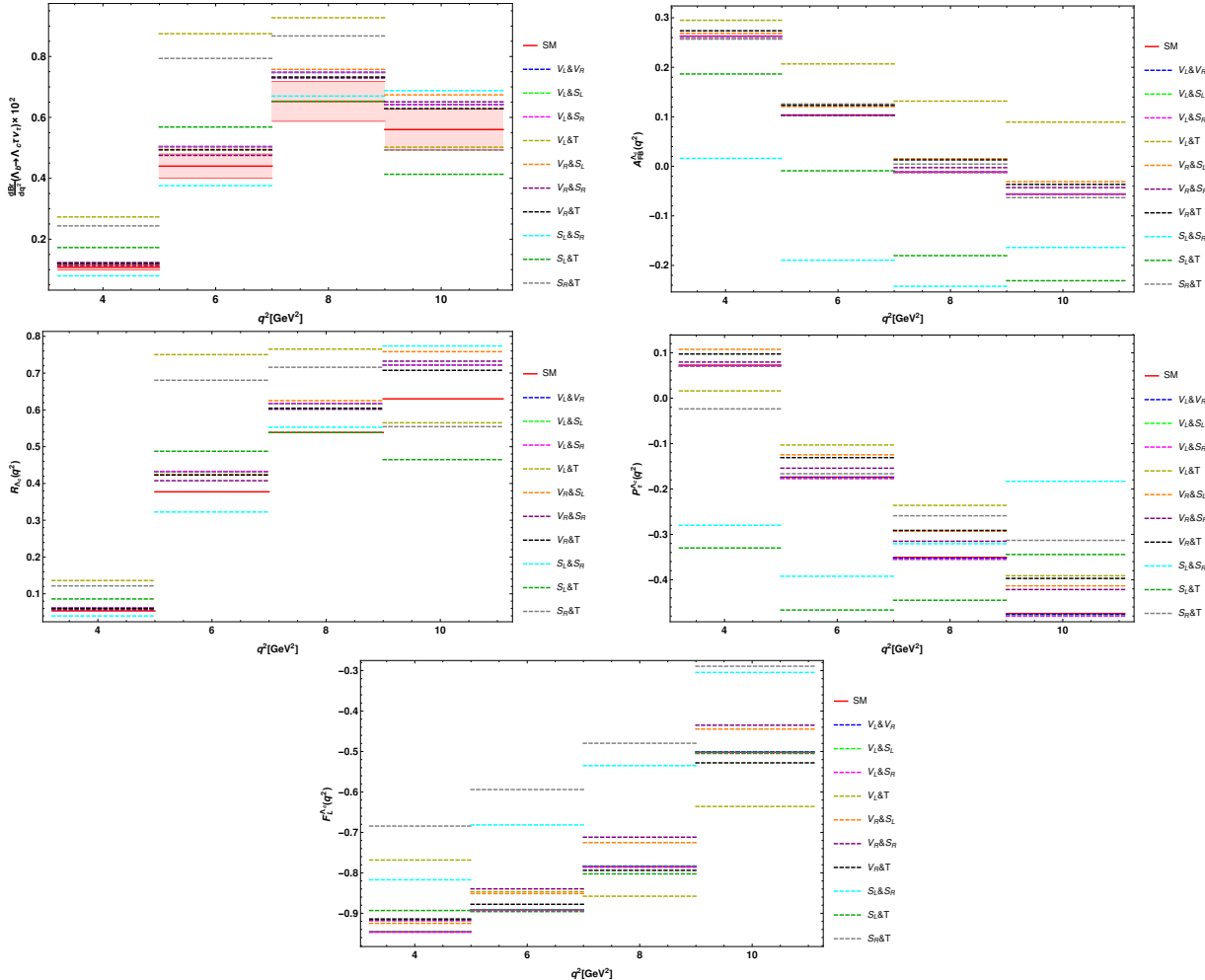


FIG. 21: The bin-wise branching ratio (top-left panel), forward-backward asymmetry (top-right panel),  $R_{\Lambda_c}$  (middle-left panel), longitudinal  $\tau$  (middle-right panel) and  $\Lambda_c$  (bottom panel) polarization asymmetry of  $\Lambda_b \rightarrow \Lambda_c \tau \bar{\nu}_\tau$  in four  $q^2$  bins for case C.

- [11] R. Aaij et al. (LHCb), Phys. Rev. Lett. **115**, 111803 (2015), [Erratum: Phys. Rev. Lett. 115, no. 15, 159901 (2015)], 1506.08614.
- [12] R. Aaij et al. (LHCb), Phys. Rev. **D97**, 072013 (2018), 1711.02505.
- [13] R. Aaij et al. (LHCb), Phys. Rev. Lett. **120**, 171802 (2018), 1708.08856.
- [14] J. P. Lees et al. (BaBar), Phys. Rev. Lett. **109**, 101802 (2012), 1205.5442.
- [15] J. P. Lees et al. (BaBar), Phys. Rev. **D88**, 072012 (2013), 1303.0571.
- [16] Heavy Flavor Averaging Group (2019), URL <https://hflav-eos.web.cern.ch/hflav-eos/semi/spring19/html/RDsDsstar/RDRDs.html>.
- [17] C. Bobeth, G. Hiller, and G. Piranishvili, JHEP **12**, 040 (2007), 0709.4174.
- [18] B. Capdevila, A. Crivellin, S. Descotes-Genon, J. Matias, and J. Virto, JHEP **01**, 093 (2018), 1704.05340.
- [19] H. Na, C. M. Bouchard, G. P. Lepage, C. Monahan, and J. Shigemitsu (HPQCD), Phys. Rev.

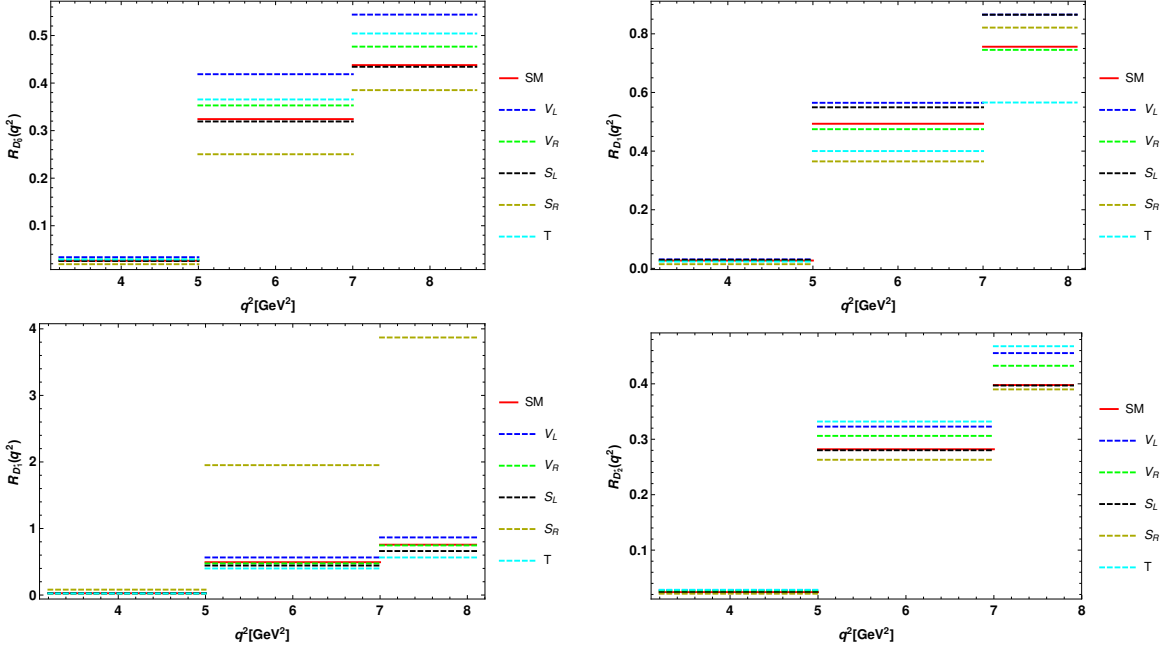


FIG. 22: The bin-wise graphical representation of  $R_{D_0^*}$  (top-left panel),  $R_{D_1}$  (top-right panel),  $R_{D_1^*}$  (bottom-left panel) and  $R_{D_2^*}$  (bottom-right panel) parameters for case A.

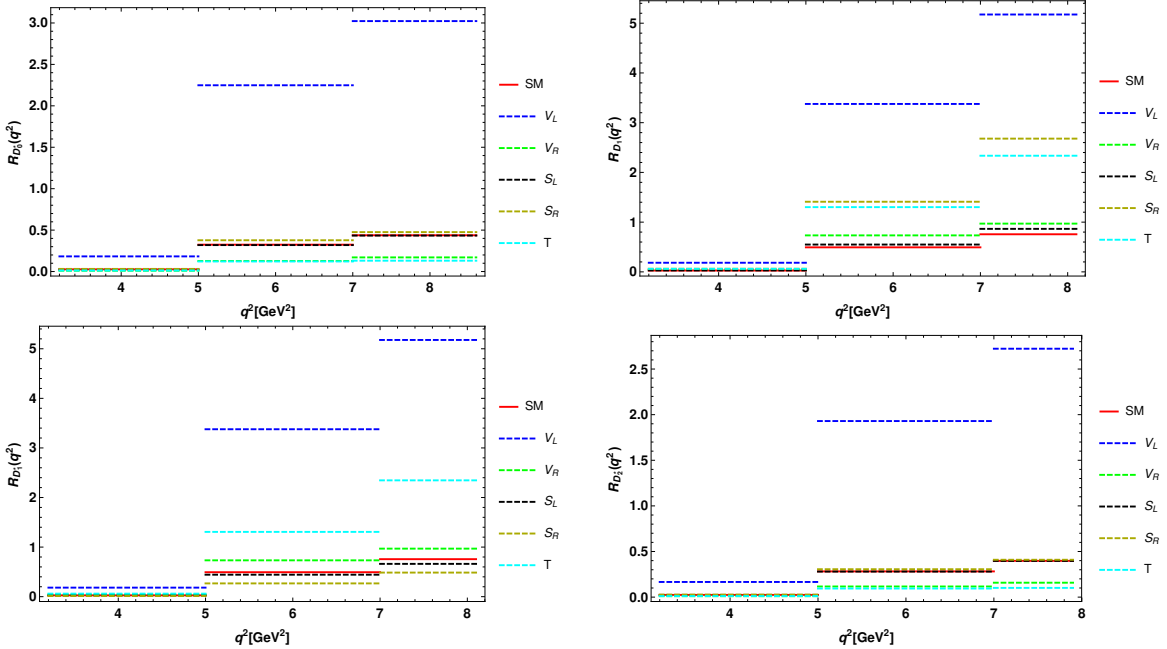


FIG. 23: The bin-wise graphical representation of  $R_{D_0^*}$  (top-left panel),  $R_{D_1}$  (top-right panel),  $R_{D_1^*}$  (bottom-left panel) and  $R_{D_2^*}$  (bottom-right panel) parameters for case B.

**D92**, 054510 (2015), [Erratum: Phys. Rev.D93,no.11,119906(2016)], 1505.03925.

[20] S. Fajfer, J. F. Kamenik, and I. Nisandzic, Phys. Rev. **D85**, 094025 (2012), 1203.2654.

[21] S. Fajfer, J. F. Kamenik, I. Nisandzic, and J. Zupan, Phys. Rev. Lett. **109**, 161801 (2012), 1206.1872.

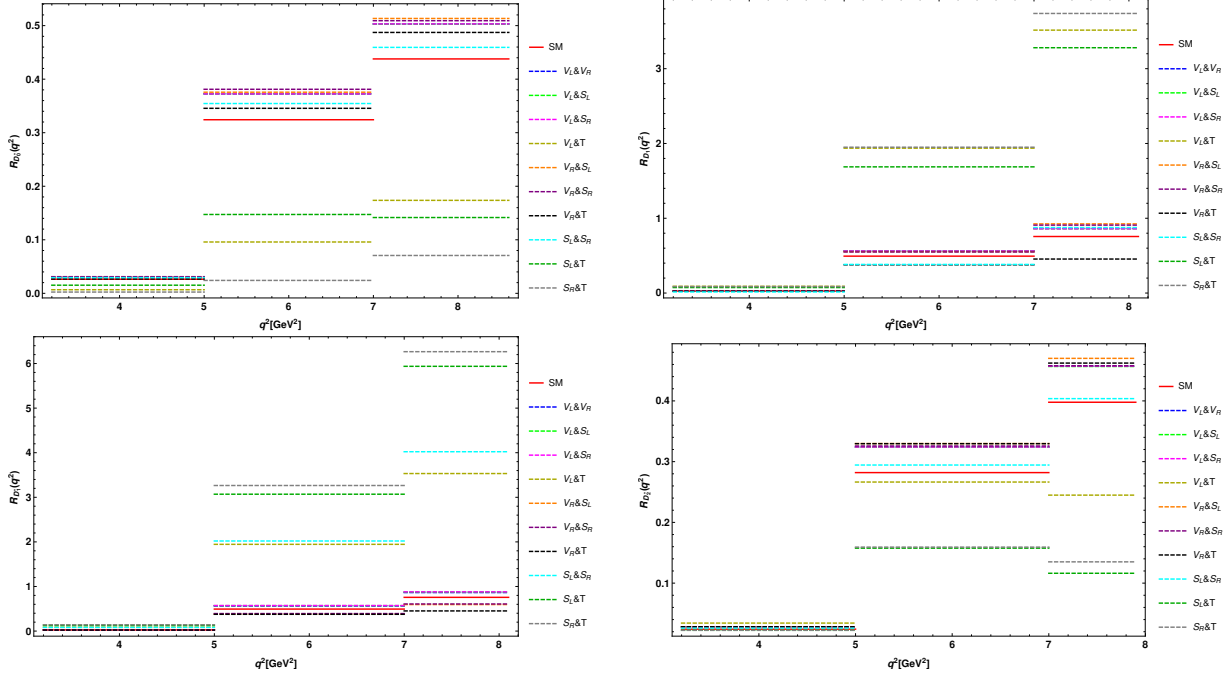


FIG. 24: The bin-wise graphical representation of  $R_{D_0^*}$  (top-left panel),  $R_{D_1}$  (top-right panel),  $R_{D_1^*}$  (bottom-left panel) and  $R_{D_2^*}$  (bottom-right panel) parameters for case C.

- [22] W.-F. Wang, Y.-Y. Fan, and Z.-J. Xiao, Chin. Phys. **C37**, 093102 (2013), 1212.5903.
- [23] M. A. Ivanov, J. G. Korner, and P. Santorelli, Phys. Rev. **D71**, 094006 (2005), [Erratum: Phys. Rev.D75,019901(2007)], hep-ph/0501051.
- [24] R. Dutta and A. Bhol, Phys. Rev. **D96**, 076001 (2017), 1701.08598.
- [25] M. Tanaka and R. Watanabe, Phys. Rev. **D87**, 034028 (2013), 1212.1878.
- [26] K. Adamczyk (Belle, Belle-II), in *10th International Workshop on the CKM Unitarity Triangle (CKM 2018) Heidelberg, Germany, September 17-21, 2018* (2019), 1901.06380.
- [27] A. Abdesselam et al. (Belle), in *10th International Workshop on the CKM Unitarity Triangle (CKM 2018) Heidelberg, Germany, September 17-21, 2018* (2019), 1903.03102.
- [28] A. K. Alok, D. Kumar, S. Kumbhakar, and S. U. Sankar, Phys. Rev. **D95**, 115038 (2017), 1606.03164.
- [29] A. Bhol, EPL **106**, 31001 (2014).
- [30] R.-H. Li, C.-D. Lu, and Y.-M. Wang, Phys. Rev. **D80**, 014005 (2009), 0905.3259.
- [31] G. Li, F.-l. Shao, and W. Wang, Phys. Rev. **D82**, 094031 (2010), 1008.3696.
- [32] M. Atoui, D. Becirevic, V. Mornas, and F. Sanfilippo, PoS **LATTICE2013**, 384 (2014), 1311.5071.
- [33] M. Atoui, V. Mornas, D. Bećirević, and F. Sanfilippo, Eur. Phys. J. **C74**, 2861 (2014), 1310.5238.

- [34] J. A. Bailey et al., Phys. Rev. **D85**, 114502 (2012), [Erratum: Phys. Rev.D86,039904(2012)], 1202.6346.
- [35] C. J. Monahan, H. Na, C. M. Bouchard, G. P. Lepage, and J. Shigemitsu, PoS **LAT-TICE2016**, 298 (2016), 1611.09667.
- [36] H. Na, C. J. Monahan, C. T. H. Davies, R. Horgan, G. P. Lepage, and J. Shigemitsu, Phys. Rev. **D86**, 034506 (2012), 1202.4914.
- [37] C. J. Monahan, C. M. Bouchard, G. P. Lepage, H. Na, and J. Shigemitsu, Phys. Rev. **D98**, 114509 (2018), 1808.09285.
- [38] X. J. Chen, H. F. Fu, C. S. Kim, and G. L. Wang, J. Phys. **G39**, 045002 (2012), 1106.3003.
- [39] Y.-Y. Fan, W.-F. Wang, and Z.-J. Xiao, Phys. Rev. **D89**, 014030 (2014), 1311.4965.
- [40] C. J. Monahan, H. Na, C. M. Bouchard, G. P. Lepage, and J. Shigemitsu, Phys. Rev. **D95**, 114506 (2017), 1703.09728.
- [41] R. Dutta and N. Rajeev, Phys. Rev. **D97**, 095045 (2018), 1803.03038.
- [42] R. Aaij et al. (LHCb), Nature Phys. **11**, 743 (2015), 1504.01568.
- [43] M. Fiore, in *Proceedings, Meeting of the APS Division of Particles and Fields (DPF 2015): Ann Arbor, Michigan, USA, 4-8 Aug 2015* (2015), 1511.00105.
- [44] C. Patrignani et al. (Particle Data Group), Chin. Phys. **C40**, 100001 (2016).
- [45] Y. K. Hsiao and C. Q. Geng, Eur. Phys. J. **C77**, 714 (2017), 1705.00948.
- [46] R. M. Woloshyn, PoS **Hadron2013**, 203 (2013).
- [47] W. Wu, Master's thesis, Mississippi U. (2015), 1505.03418, URL <http://search.proquest.com/docview/1697862095>.
- [48] S. Shivashankara, W. Wu, and A. Datta, Phys. Rev. **D91**, 115003 (2015), 1502.07230.
- [49] T. Gutsche, M. A. Ivanov, J. G. Korner, V. E. Lyubovitskij, and P. Santorelli, Phys. Rev. **D93**, 034008 (2016), 1512.02168.
- [50] T. Gutsche, M. A. Ivanov, J. G. Krner, V. E. Lyubovitskij, P. Santorelli, and N. Habyl, Phys. Rev. **D91**, 074001 (2015), [Erratum: Phys. Rev.D91,no.11,119907(2015)], 1502.04864.
- [51] W. Detmold, C. Lehner, and S. Meinel, Phys. Rev. **D92**, 034503 (2015), 1503.01421.
- [52] R. Dutta, Phys. Rev. **D93**, 054003 (2016), 1512.04034.
- [53] M. Pervin, W. Roberts, and S. Capstick, Phys. Rev. **C72**, 035201 (2005), nucl-th/0503030.
- [54] R. N. Faustov and V. O. Galkin, Eur. Phys. J. **C76**, 628 (2016), 1610.00957.
- [55] A. Datta, S. Kamali, S. Meinel, and A. Rashed, JHEP **08**, 131 (2017), 1702.02243.
- [56] X.-Q. Li, Y.-D. Yang, and X. Zhang, JHEP **02**, 068 (2017), 1611.01635.
- [57] E. Di Salvo, F. Fontanelli, and Z. J. Ajaltouni (2018), 1804.05592.

- [58] F. U. Bernlochner, Z. Ligeti, D. J. Robinson, and W. L. Sutcliffe (2018), 1808.09464.
- [59] A. Ray, S. Sahoo, and R. Mohanta, Phys. Rev. **D99**, 015015 (2019), 1812.08314.
- [60] F. U. Bernlochner and Z. Ligeti, Phys. Rev. **D95**, 014022 (2017), 1606.09300.
- [61] F. U. Bernlochner, Z. Ligeti, and D. J. Robinson, Phys. Rev. **D97**, 075011 (2018), 1711.03110.
- [62] Y. Sakaki, M. Tanaka, A. Tayduganov, and R. Watanabe, Phys. Rev. **D88**, 094012 (2013), 1309.0301.
- [63] P. Biancofiore, P. Colangelo, and F. De Fazio, Phys. Rev. **D87**, 074010 (2013), 1302.1042.
- [64] J. A. Bailey et al. (MILC), Phys. Rev. **D92**, 034506 (2015), 1503.07237.
- [65] I. Caprini, L. Lellouch, and M. Neubert, Nucl. Phys. **B530**, 153 (1998), hep-ph/9712417.
- [66] J. A. Bailey et al. (Fermilab Lattice, MILC), Phys. Rev. **D89**, 114504 (2014), 1403.0635.
- [67] Y. Amhis et al. (Heavy Flavor Averaging Group (HFAG)) (2014), 1412.7515.
- [68] T. Kurimoto, H.-n. Li, and A. I. Sanda, Phys. Rev. **D67**, 054028 (2003), hep-ph/0210289.
- [69] R. Watanabe, Phys. Lett. **B776**, 5 (2018), 1709.08644.
- [70] S. Aoki et al., Eur. Phys. J. **C74**, 2890 (2014), 1310.8555.
- [71] T.-W. Chiu, T.-H. Hsieh, C.-H. Huang, and K. Ogawa (TWQCD), Phys. Lett. **B651**, 171 (2007), 0705.2797.
- [72] M. Tanabashi et al. (Particle Data Group), Phys. Rev. **D98**, 030001 (2018).
- [73] A. G. Akeroyd and C.-H. Chen, Phys. Rev. **D96**, 075011 (2017), 1708.04072.
- [74] Z.-R. Huang, Y. Li, C.-D. Lu, M. A. Paracha, and C. Wang, Phys. Rev. **D98**, 095018 (2018), 1808.03565.
- [75] A. Ray, S. Sahoo, and R. Mohanta, Eur. Phys. J. **C79**, 670 (2019), 1907.13586.